

# Experimental Study of the Shear Strength of Bonded Concrete–Rock Interfaces: Surface Morphology and Scale Effect

Hussein Mouzannar<sup>1</sup>  · Marion Bost<sup>1</sup> · Madly Leroux<sup>2</sup> · Didier Virely<sup>3</sup>

Received: 18 March 2016 / Accepted: 5 June 2017 / Published online: 22 June 2017  
© Springer-Verlag GmbH Austria 2017

**Abstract** The shear strength of the concrete–rock interface is a key factor to justify the stability of a hydraulic structure foundation. The Mohr–Coulomb failure criterion is usually used as shear strength and evaluated by extrapolating shear tests results carried out in a laboratory on small-sized samples. This paper presents an experimental study on the concrete–rock interface shear behavior. The effect of rock surface morphology on shear behavior was studied by performing laboratory direct shear tests on prepared square samples with a previously characterized rock surface. The scale effect and the test conditions were also studied by comparing the results to those obtained by performing usual laboratory shear tests on cored samples at lower scale. The tested interfaces were composed of the same concrete and granite and have a natural rock surface. The results displayed that the peak shear strength is strongly dependent on the concrete–rock bonding, the rock surface morphology and the applied normal load. A new surface morphology description tool was developed in order to characterize the main waviness. Moreover, the concrete–rock shear behavior at medium scale was reproduced by a 2D finite elements model to study the stress distribution along the sheared interface. Under low normal load, the concrete–rock adhesion is thus progressively

mobilized according to the waviness on the rock surface and the local shear failure mechanisms depend on the type of this main waviness. Consequently the shear strength of a concrete–rock interface must be analyzed with respect to the various morphology aspects on its rock surface.

**Keywords** Concrete–rock interface · Shear strength · Surface morphology · Scale effect · Direct shear test

## 1 Introduction

The design for new hydraulic structures such as gravity dams requires evaluating the sliding stability along the foundation concrete–rock interface. Existing concrete gravity dams also need this safety reassessment to evaluate their compliance with modern regulatory rules (Krounis et al. 2015). Different methods are used worldwide to justify the sliding stability of a dam foundation at concrete–rock contact. The methods differ by the chosen load combination and the evaluation of shear strength. In general, the shear strength is expressed by a Mohr–Coulomb failure criterion referring to the failure line defined by both friction angle ( $\varphi$ ) and cohesion ( $c$ ) parameters (Ruggeri et al. 2004; CFBR 2013; Westberg Wilde and Johansson 2013). However, if the applied loads are well known (hydraulic loads, uplift pressure, dam weight), the shear strength parameters are difficult to estimate.

The shear strength of the concrete–rock interface is usually obtained by performing laboratory shear tests on samples of small size relative to that of a gravity dam foundation. However, CFBR (2013) observed that the values of the characteristic parameters thus obtained are different from the values evaluated in situ: The friction angle and cohesion are, respectively, higher and lower at

✉ Hussein Mouzannar  
hussein.mouzannar@hotmail.com

<sup>1</sup> Geotechnical Engineering, Environment, Natural Hazards and Earth Sciences Department, IFSTTAR, 69675 Bron, France

<sup>2</sup> Technical Department for Geological, Geotechnical and Civil Engineering Testing, EDF, 13097 Aix-en-Provence, France

<sup>3</sup> Direction territoriale Sud-Ouest, CEREMA, 31073 Toulouse, France

real scale than the values obtained in the laboratory. For the friction angle, it is justified by the fact that the morphology of the contact at real scale displays significant irregularities created by the rock foundation excavation which cannot be considered at laboratory scale. For the cohesion, the main reason given is that only the cohesion of the bonded samples can be measured. This value measured in the laboratory should therefore be weighted with the proportion of bonded contact area compared to the base area of the dam. Thus, during the gravity dam foundation conception and for safety reasons, the cohesion is currently assessed to be null and the laboratory safe value is given to the friction angle. These evaluation methods lead to a conservative estimation of the concrete–rock interface shear strength which is no longer suitable for new demands of safety level.

The objective of this study is to improve the shear strength assessment of the concrete–rock interface of a gravity dam. The concrete–rock shear strength is first reviewed. Then a series of direct shear tests performed on different sample sizes having similar concrete–rock contacts are presented. The rock surfaces were natural granite surfaces. Tensile tests on contacts complete this experimental study. A new morphology characterization tool is proposed in order to characterize the rock surface waviness; then, a 2D finite elements model is implemented to reproduce the shear behaviors at medium scale taking into account the morphology effect. Results are discussed with regard to the surface morphology, the size sample and the testing conditions in order to propose a more accurate assessment of the interface shear strength in a laboratory.

## 2 Shear Strength of the Bonded Concrete–Rock Interface

Several researches (EPRI 1992; Saiang et al. 2005; Moradian 2011; Gutiérrez 2013; Krounis et al. 2016) attempted to study the shear behavior of concrete–rock interfaces using experimental approaches. Experimental studies were mainly based on direct shear tests (Fig. 1). Sometimes as in the case of Lo et al. (1990), the concrete–rock interface shear strength was evaluated by performing triaxial tests. Moreover, direct tensile tests were carried out on concrete–rock contacts to assess the bonding value between concrete and rock (Bauret and Rivard 2015).

Direct shear tests within concrete–rock interfaces in these studies were performed mainly on samples cored from an existing concrete–rock interface (Lo et al. 1990; EPRI 1992) or on laboratory-prepared interfaces (Moradian 2011; Tian et al. 2015). Most tests were carried out on samples of dimensions smaller than those of dam foundations (Ruggeri et al. 2004). The experimental results

showed that the concrete–rock interface shear strength is influenced by the following factors:

- the initial cohesion between concrete and rock (Lo et al. 1990; Moradian et al. 2012),
- the rock surface morphology (Kodikara and Johnston 1994; Saiang et al. 2005; Gutiérrez 2013; Champagne et al. 2013),
- the mechanical properties of rock and concrete (EPRI 1992),
- the applied normal stress (Moradian et al. 2012; Tian et al. 2015).

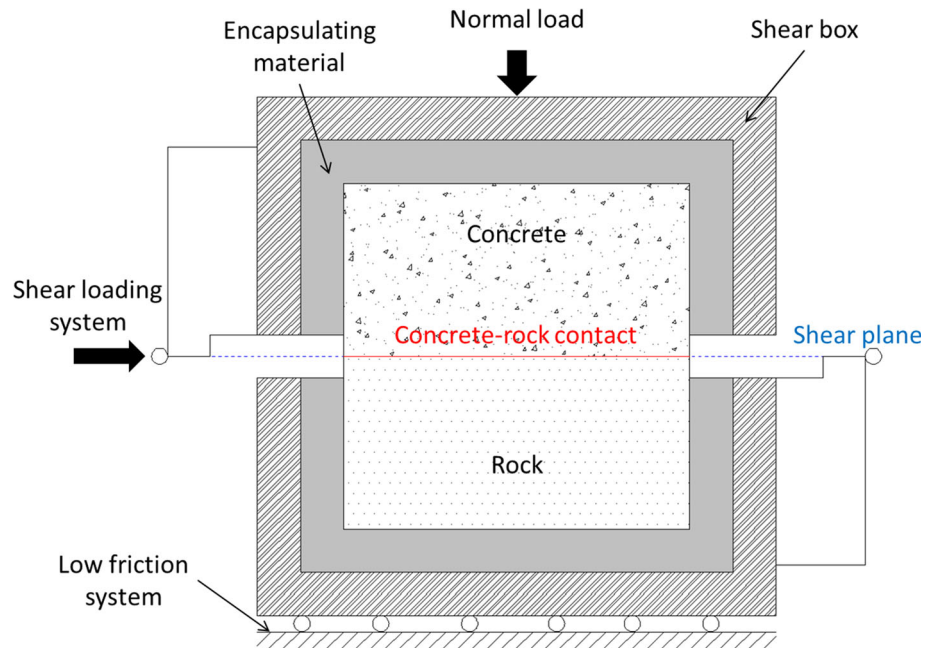
In rock mechanics, it is admitted that the rock roughness has a significant impact on the shear characteristics of rock joints. In response, several shear failure criteria for rock–rock interfaces were established taking into account the effect of the rock surface morphology on the interface shear strength (Patton 1966; Barton and Choubey 1977; Maksimovic 1996; Grasselli 2001; Johansson 2009). However, these models do not take into account the role of bonding between rock and concrete at the beginning of the failure. Lo et al. (1991) attempted to develop a shear failure criterion for a concrete–rock interface by evaluating the shear strength as the sum of the well-bonded concrete–rock contact shear strength and unbonded concrete–rock contact shear strength.

Furthermore, some in situ direct shear tests on concrete–rock interface were also carried out to study the concrete gravity dam foundation (Ghosh 2010; Barla et al. 2011). However, due to difficulties of performing in situ tests and their expensive cost, the number of in situ tests performed on concrete–rock interfaces is limited. Moreover, the accurate evaluation of the effective shear strength of the concrete–rock interface needs to consider the deformation of the rock mass which is unknown (Andjelkovic et al. 2015).

Studies of the scale effect on the shear behavior within rock discontinuities showed the influence of sample size on the rock–rock interface shear behavior (Barton and Choubey 1977; Bandis et al. 1981; Castelli et al. 2001; Fardin et al. 2003; Tatone and Grasselli 2012). This effect appears to depend on the conditions of the direct shear test (shear plane, shear rate, normal stress) and the type of rock surface (natural, artificial or flat surface). Moreover, these results do not consider the particular case of the concrete–rock interface for which there is an initial adhesion between concrete and rock.

At last, according to most of the national guidelines, to assess the safety against sliding for a gravity dam, limit equilibrium methods modeling the dam as a rigid body allowed to slide along its base are used with the shear strength of concrete–rock interface expressed by a Mohr–Coulomb failure criterion (Ruggeri et al. 2004). The shear strength is thus established by integrating the normal stress

**Fig. 1** Schematic illustrating arrangement of specimen in a laboratory direct shear test



over the entire potential sliding plane assuming the shear stress to be homogenous on the entire shear surface and the shear strength to be simultaneously mobilized at the time of failure. According to Krounis et al. (2015), this assumption leads to overestimate, significantly, the effective shear strength of the interface. In fact, according to Westberg Wilde and Johansson (2013), there is a spatial variation in bond strength between concrete and rock due to the rock surface cleanness before concrete casting, the local rock quality and the position of leakage on the contact. This possible spatial variation in adhesion introduces weak areas where the failure process can be initiated and therefore a progressive mechanism of failure.

### 3 Methodology for the Experimental Study of the Rock–Concrete Interface

The shear strength of the bonded concrete–rock interface was studied experimentally in order to investigate the influence of rock surface morphology and the scale effect.

#### 3.1 Description

A series of direct shear tests at two different scales (Table 1) were performed under experimental conditions as

similar as possible to those of a concrete gravity dam. In addition, direct tensile tests were carried out on a similar concrete–rock interface in order to evaluate the tensile strength of the contact.

The same concrete and rock were used for all samples. The rock type used for the tests was granite: Large granite rock blocks were sampled in the same quarry in France (Corrèze), each one having an unweathered natural surface. The selected granite has a uniaxial compressive strength of 133 MPa (10 tested samples, CV—coefficient of variation = 5.90%) and a tensile strength of 10.20 MPa (5 tested samples, CV = 13.90%). The mixture of concrete used in this study shown in Table 2 was chosen on the basis of an analysis of that of existing French concrete gravity dams. This composition provides a standard compressive strength of 43.4 MPa (9 tested samples from 3 different pouring phases, CV = 1.60%) and a tensile strength of 3.75 MPa (9 tested samples from 3 different pouring phases, CV = 7.10%).

#### 3.2 Rock Surface Morphology Characterization

To study the rock surface morphology effect and to position the shear plane relative to the mean plan of the rock surface, the rock surface morphology was characterized for each tested sample.

**Table 1** Samples for the direct shear tests

Scale	Shape	Dimensions (m)	Shear surface (m <sup>2</sup> )	Number of samples
Medium	Square	0.18 × 0.18	0.0324	9
Small	Cored	D = 0.08	0.0050	8

**Table 2** Used mixture for concrete

Ingredient	Ratio (kg/m <sup>3</sup> )
Concrete	280
Sand 0/4 mm	650
Washed sand 0/2 mm	150
Crushed stone 11.2/22.4 mm	780
Crushed stone 4/11 mm	330
Adjuvant—OPT 203	2.80
Water	157

The sample rock surfaces were first digitized using a device measuring the height of the irregularities compared to a reference plane. A 3D stereotopometric measurement system, called the ATOS Compact Scan and manufactured by the GOM company, was chosen as it meets our requirements: in situ measurement, capacity for large area measurement, high accuracy and resolution. The ATOS compact scan system consists of a measurement head containing a central projector unit of structured light fringe patterns and two CCD cameras, and a PC to pilot the system. The used sensors of the ATOS apparatus and the measurement distance were chosen to give an average spacing between the measurement points of 0.25 mm and a measurement accuracy about 0.01 mm.

The topography of each rock surface sample was reproduced by means of these measurements. Thus, the mean plane of each digitized rock surface was calculated using the least square method based on the obtained 3D coordinates. The rock surface morphology was then displayed relative to this mean plane.

To characterize and compare quantitatively the rock surface morphologies of samples, some usual roughness parameters (statistical and three-directional parameters) were calculated:

- $Z_2$  is the root mean square (RMS) of the first derivate of the altitudes (Myers 1962);
- $k$  is the difference between the maximum and the minimum altitudes over the whole rock surface (Gentier 1987);
- $R_s$  is the ratio of the true surface area to its nominal surface area (El-Soudani 1978);
- $\frac{\theta_{\max}^*}{(C+1)}$  is a 3D parameter given by Tatone and Grasselli (2009) which characterizes the distribution of the inclination and orientation of each triangular facet of a TIN<sup>1</sup> surface:  $\theta_{\max}^*$  is the maximal facet inclination

<sup>1</sup> Triangulated irregular network (Grasselli 2001).

compared to the mean plane and  $C$ , a fitted parameter. Tatone and Grasselli (2009) give more details about this 3D parameter.

Tables 3 and 4 summarize these values assessed on each rock surface sample tested at small and medium scales, respectively, and their average and coefficient of variation (CV). Given the low values of the calculated coefficient of variation, except for  $Z_2$  at medium scale (57.76%), and according to the physical meaning of these parameters, the rock surfaces at each scale have a similar roughness characterization. On the contrary, we can emphasize the important variations of the calculated average values between the two different scales (CV = 27% for  $Z_2$ , 43% for  $k$  and 54% for  $\frac{\theta_{\max}^*}{(C+1)}$ ). These variations point out that the rock surface morphology is itself submitted to scale effect.

**Table 3** Some roughness parameters for the rock surface of the cored samples tested at small scale (0.08-m-diameter circular surfaces)

Core sample	$Z_2$	$k$ (mm)	$R_s$	$\frac{\theta_{\max}^*}{(C+1)}$
H1	0.2707	7.58	1.0678	11.3126
H2	0.2613	7.78	1.0670	12.2655
H3	0.2924	7.82	1.0811	12.1374
H4	0.2553	9.56	1.0672	11.1518
H5	0.2423	8.42	1.0606	10.3536
H6	0.2590	9.45	1.0640	11.7393
H7	0.2555	8.30	1.0714	11.3031
H8	0.2594	7.41	1.0706	11.3897
Average	0.2620	8.23	1.0687	11.4566
CV (%)	5.39	10.84	0.57	5.34

**Table 4** Some roughness parameters for the rock surface of the samples tested at medium scale (0.18 m × 0.18 m square surfaces)

Square sample	$Z_2$	$k$ (mm)	$R_s$	$\frac{\theta_{\max}^*}{(C+1)}$
T1	0.2193	12	1.0343	6.9275
T2	0.1594	15	1.0225	6.0540
T3	0.6170	13	1.0184	6.1320
T4	0.2646	11	1.0180	5.5426
T5	0.4723	13	1.0183	5.9312
T6	0.6693	14.5	1.0275	7.1276
T7	0.1923	12.5	1.0298	8.5221
T8	0.1410	12	1.0189	6.0958
T9	0.3699	12.5	1.0257	7.0350
Average	0.3450	12.80	1.0237	6.5964
CV (%)	57.76	9.74	0.57	13.77

### 3.3 Sample Preparation

To achieve a correct adhesion between concrete and rock like for building a gravity dam, each rock surface was cleaned carefully with a water high-pressure cleaner before the surface topography measurement and the concrete pouring. As the chosen granite rock surfaces were unweathered, the water high-pressure cleaner had a limited impact on the rock surfaces morphology.

After the rock surface digitalization, the rock surface topography appearances were compared visually and the shear direction on each surface was determined in order to obtain variability on the rock surface morphology of the interfaces tested under the same normal stress (morphologies having one central crest on the rock surface or morphologies having different crests distributed on the rock surface).

All concrete–rock samples were prepared in a laboratory. The tests on samples were performed after 28 days of concrete hardening. The preparation procedure for each scale is described in detail as follows.

#### 3.3.1 Square Samples for Direct Shear Test at Medium Scale

The direct shear tests on the square samples at medium scale were performed with the MTS 816 loading system (Fig. 2) of the CEREMA (Center for Expertise and Engineering on Risks, Urban and Country Planning, Environment and Mobility) rock mechanics laboratory (Toulouse, France). The loading rigid frame consists of a platform for shear test with a two-part shear box. The maximum normal and tangential loads are 500kN and 200kN, respectively. The displacement of the boxes to each other is measured and recorded by 4 vertical linear variable displacement transformers (LVDTs) on each edge of the box for the normal displacement and by 2 additional lateral LVDTs for the tangential displacement in the shearing direction.

To facilitate the setting of the concrete–rock interface in the shear plane of the shear box, it was decided to prepare the sample having a shear surface smaller than that of the used loading system ( $0.2 \times 0.2 \text{ m}^2$ ). For this purpose, 9 cuboid rock blocks having 0.18 m length, 0.18 m width and 0.1 m as average height were machined from one original large granite block leaving on each small block a face having a natural rough surface as shown in Fig. 3.

Using the digitization of the natural surface of the granite blocks (Sect. 3.2), the mean planes were then calculated and marked on the blocks.

To cast the concrete, film-faced plywoods were used for formworks. Their upper level was adjusted so that the distance between the upper level of the plywoods and the mean plane was equal to 0.1 m. Then, concrete was cast

and vibrated on the rock blocks. After 7 days of hardening, the formwork was removed and the mean plane of rock surface was marked on the four lateral faces of each sample in order to define the mean plane for the next step of the sample preparation (Fig. 4).

Afterward the sample was placed in the shear box of the load apparatus. The sample was centered in the box in such a way that the mean plane of the rock surface became in the midplane of the box, namely in the shear plane of the apparatus. Then the sample was fixed into the box by using a rapid-hardening mortar ( $R_c$ , compression strength = 30 MPa after 1-day hardening). This preparation was repeated for each sample at least 1 day before performing the direct shear test.

#### 3.3.2 Cored Samples for Direct Shear Test at Small Scale

The direct shear tests on the cored samples were performed with the 3R shear box system of the technical department for geology, geotechnical and civil engineering testing (TEGG) of EDF (French Electricity Company, Aix-en-Provence, France). As shown in Fig. 5, the apparatus consists of a static lower box and a mobile upper box. The system can apply normal and shear loads up to 30 and 50 kN, respectively. The normal and tangential displacements are measured via one LVDT for each displacement direction.

In order to get samples with the same characteristics of concrete and rock for all direct shear tests, an artificial concrete–rock interface was prepared in the laboratory, and then, the samples were drilled from it. To obtain this artificial interface, a 0.15 m layer of concrete was cast on a granite block from the same quarry as for the granite blocks for square samples (Sect. 3.3.1). The block had a natural rock surface of  $0.9 \times 0.75 \text{ m}^2$ . Before concrete pouring, the whole rock surface was digitized with the ATOS compact scan system. The core drilling positions were defined (Fig. 6) considering a minimum distance (150 mm) between each core to overcome the boundary effects during the drilling process. The coordinates of each core center were then plotted on the block lateral sides in order to reposition the cores center on the top surface of the concrete after pouring. The rock surface topography of each cored rock surface was exported in order to characterize the surface morphology as presented in Sect. 3.2.

After 15 days of concrete hardening, the 8 samples were drilled with a 0.08-m-diameter diamond-drilling unit with water lubrication. All the cored samples were extracted without any visible damage on the contact. Using the digitized topography, the rock surface mean plane of each cored sample was calculated and marked on the cored sample.



**Fig. 2** MTS 816 direct shear test apparatus (adapted from MTS 2014) used for the medium scale samples

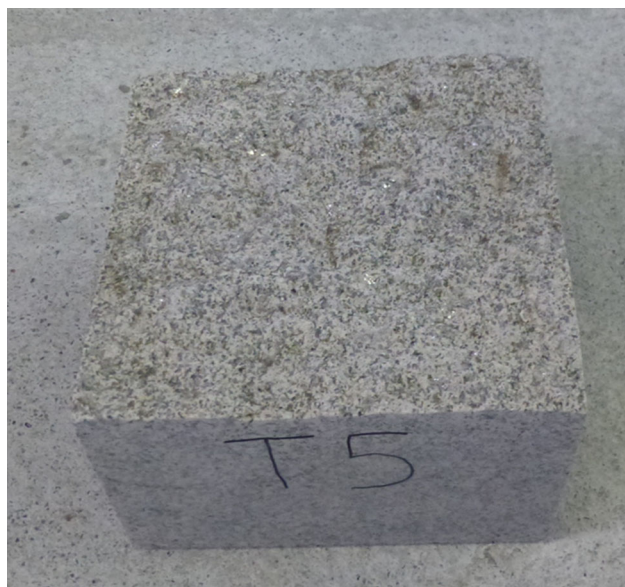
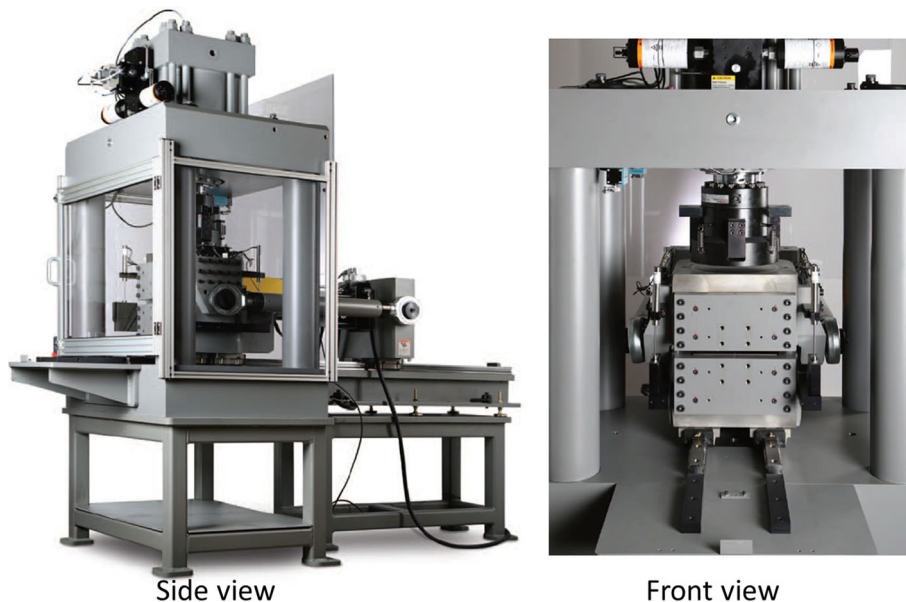


**Fig. 3** A rock block used for a square sample preparation

The French standard (XP P 94-424) was respected to prepare the samples in order to use the same procedure as that of samples cored from existing dams. The drilled cores were cut to have the height of the shear box (Fig. 7) and placed in a steel mold having the same dimensions as the shear box. The cored samples were centered in the molds in such a way that the marked mean plane was located in the midplane of the mold, i.e., the shear plane of apparatus. The cored samples were thereafter encapsulated in the molds with rapid-hardening mortar ( $R_c$ , compression strength = 20 MPa after 1-day hardening). A typical final direct shear test sample, grouted in mortar and ready for testing, is shown in Fig. 8.

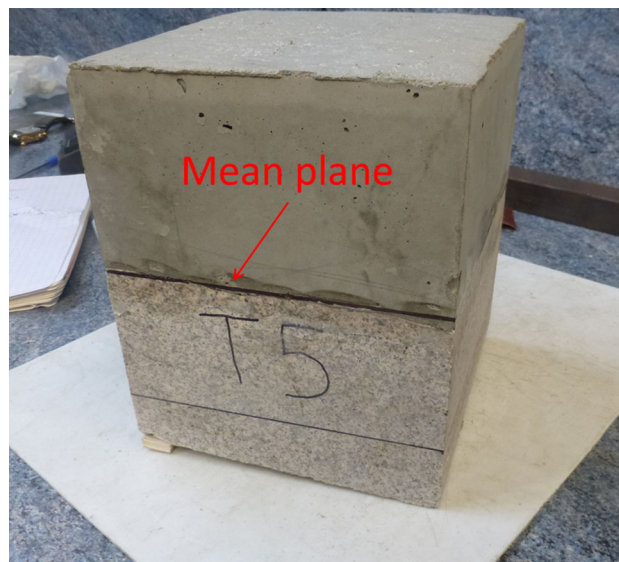


**Fig. 4** A square sample before encapsulating into the shear box

### 3.3.3 Cylindrical Samples for Direct Tensile Test

An artificial concrete–rock interface was prepared in the laboratory. To obtain this artificial interface, a 0.15 m layer of concrete was cast on a granite block taken from the same quarry as the granite blocks for square samples (Sect. 3.3.1). This block had a surface of  $1 \times 1 \text{ m}^2$ . After 15 days of concrete hardening, the block was drilled in various places with a diamond-drilling unit having a diameter of 0.148 m, making sure that the drilling core exceeded the concrete–rock interface without breaking the cored sample. A threaded rod was sealed at the center of each core perpendicular to its upper surface. Then a steel disk with a diameter of 0.145 and 0.03 m height was screwed onto the threaded rod and glued

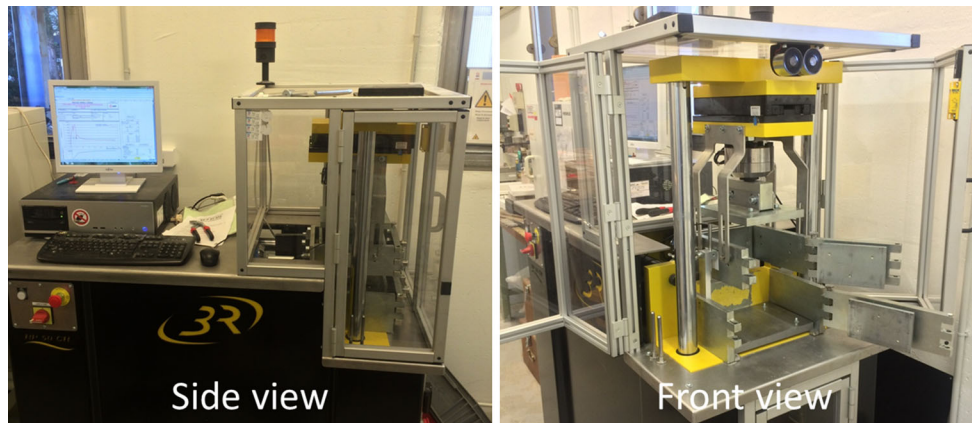


**Fig. 5** 3R direct shear test apparatus used for the small scale samples

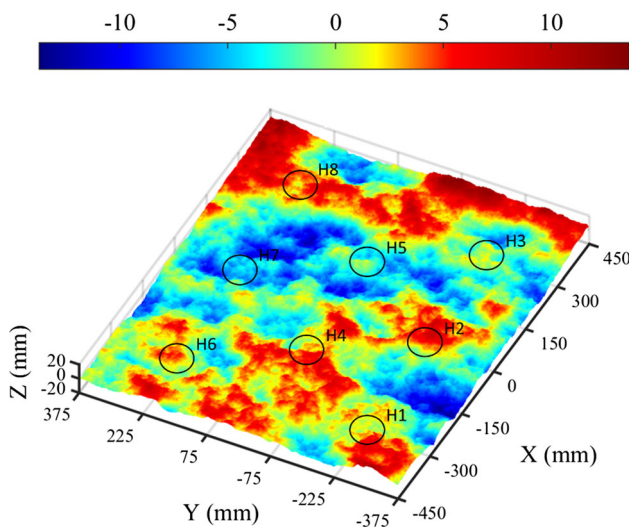


**Fig. 6** Core drilling positions on the rock surface topography

**Fig. 7** Cored samples



to the upper surface of the core. Figure 9 shows a prepared block for tensile test with also the hydraulic jack used to apply the tensile load, and the related equipment. For more details, the experimental procedure is presented in Deveze and Coubard (2015).

#### 4 Tests Results

The direct shear tests were performed under constant normal load conditions and a constant shear rate of 0.1 mm/min respecting the ISRM standard for direct shear test on rock discontinuities (Muralha et al. 2014). Furthermore, based on the estimated normal stresses to which the gravity dam foundation would be subjected, 3 normal stresses below 1 MPa were chosen for shear tests: 0.2, 0.6 and 1 MPa. This range of normal stress values was estimated



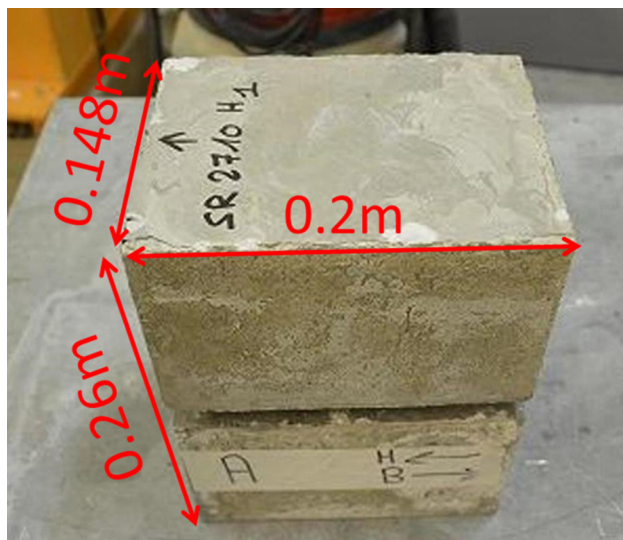


**Fig. 8** A final direct shear test sample for cored sample

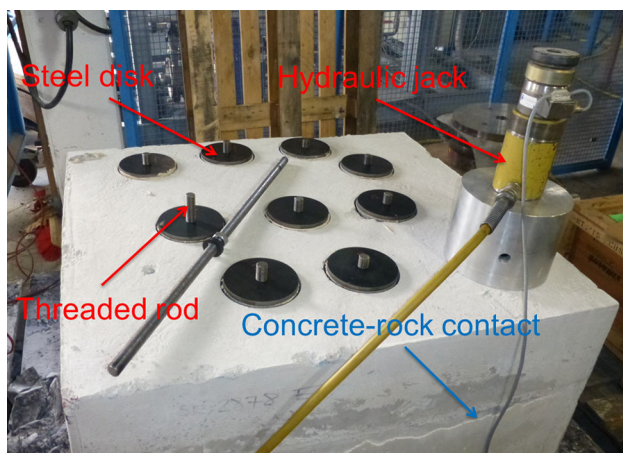


**Fig. 9** Prepared concrete-rock block for tensile test

considering usual concrete gravity dams in France, from 10 to 60 m high, made of concrete with an average unit weight of about  $2300 \text{ kg/m}^3$  (CFBR 2013).

Data were registered during the tests at a time interval of 0.1 s (10 Hz). The following presented shear and normal stresses at the interface were calculated by dividing the force values by the corrected shear area, at each instant, taking into account the shear displacement.

#### 4.1 Direct Shear Tests at Medium Scale

Nine direct shear tests were carried out under the 3 different normal load values, 0.2, 0.6 and 1 MPa. As shown in Figs. 10 and 11, the sample failure occurred well at the concrete-rock contact. The normal stress, peak shear stress, peak shear displacement and residual stress of these direct shear tests are summarized in Table 5.



**Fig. 10** Concrete surface of sample T8 after the test—the arrow indicates the shear direction



**Fig. 11** Rock surface of sample T8 after the test—the arrow indicates the shear direction

In Fig. 12a, the shear stress is observed to increase steeply until a peak value and then the shear stress drops sharply. These are typical curves of the shear behavior for bonded interface at low normal load (Ruggeri et al. 2004; Tian et al. 2015). However, after the stress peak, the shear stress as a function of shear displacement curves can be divided into two distinct shear behaviors named “A” and “B,” corresponding to two different typical curves:

- typical curve “A”—Fig. 12a: the shear stress increases steeply until the occurrence of the failure (peak shear stress). Then it drops sharply until the normal stress value, showing a sudden brittle failure. This failure was noted with an audible sound during the shear test. Thereafter, the shear stress increases again until a new peak stress is attained followed by a decreasing phase corresponding to the residual behavior,



**Table 5** Summary of the direct shear tests results at medium scale

Sample	Normal stress $\sigma_n$ (MPa)	Peak shear stress $\tau_p$ (MPa)	Type of behavior	Peak displacement $\delta_p$ (mm)	Residual stress $\tau_r$ (MPa)
T1	0.20	2.36	A	0.12	0.34
T2	0.20	1.57	B	0.10	0.25
T3	0.20	1.20	B	0.21	0.23
T4	0.60	3.72	A	0.46	0.63
T5	0.60	1.50	B	0.15	0.67
T7	0.60	3.42	A	0.16	0.63
T6	1	4.17	A	0.42	1.16
T8	1	2	B	0.31	1.05
T9	1	4.45	A	1	1.05

- typical curve “B”—Fig. 12a: The shear stress increases steeply until the occurrence of the failure (peak shear stress). The peak value is lower than that of the typical curve “A.” Then the shear stress drops sharply showing a brittle failure too but quickly followed by a gradual decrease (softening phase) until the residual behavior.

The dotted curves in Fig. 12a display the dilatancy curves during the shear tests on the samples T4 and T5. No difference was underlined between the dilatancy curves appearance of the two types A and B:

- before peak shear stress, there is no dilatancy,
- after the peak, the dilatancy increases with increasing shear displacement.

The shear displacement curves are also reported in terms of apparent friction coefficient (shear force over normal force) to figure out the influence of the real contact area on the shear behavior (Fig. 12b). In this case, the shapes of the observed curves (Fig. 12b) were found to be very similar to those of the curves representing the shear stress evaluated with the apparent shear area (Fig. 12a). Thus, regarding the results of the observed concrete–rock interface failures dimensions (Table 5), we can assume that there are no significant errors on the peak shear stress.

## 4.2 Direct Shear Tests at Small Scale

Eight direct shear tests at small scale on cored samples were conducted under the same normal load values as those at medium scale (0.2, 0.6 and 1 MPa). The cored samples failure occurred at the contact between concrete and rock (Fig. 13).

The normal stress, peak shear stress, peak shear displacement and residual stress of the 8 direct shear tests at small scale are summarized in Table 6. The peak displacement values are more important than those evaluated at medium scale. In fact, on the 3R direct shear apparatus, one single LVDT sensor fixed on the hydraulic jack which

applies the shear displacement monitors the tangential displacement. The relative tangential displacement between the two half-boxes is not directly measured. According to shear tests performed at medium scale, the values of shear displacements measured on the hydraulic jack are greater than those measured relative to the movable half-box. Therefore, the peak displacement values noted in Table 6 have not to be considered as representative of the real displacement in the concrete–rock interface at the peak stress.

The typical obtained shear stress as a function of shear displacement curve is shown in Fig. 14a. This is similar to that observed for sample of type A at medium scale described in Sect. 4.1: It corresponds to the shear behavior of a well-bonded concrete–rock interface (Gutiérrez 2013; Moradian 2011; Saiang et al. 2005; Tian et al. 2015; Ruggeri et al. 2004).

Besides, the friction coefficient is figured out as a function of shear displacement (Fig. 14b). As described before, since the shapes of the obtained curves are very similar whether in shear stress (Fig. 14a) or in friction coefficient (Fig. 14b), the shear area correction to assess the shear stresses is sufficient to represent the shear results.

## 4.3 Direct Tensile Tests

There is no standard that describes a procedure for performing a tensile test on a concrete–rock interface. The test was here controlled by a constant tensile effort rate of 25kN/min until the sample failure. The failure occurred in one of the 4 locations is shown in Fig. 15. Table 7 summarizes the results of the 11 performed direct tensile tests: The failures of 4 samples occurred away from the interface. These were excluded from the results and the average tensile strength thus obtained is about 1.22 MPa with a coefficient of variation 19%. This value is comparable to those obtained for the Lo et al. (1990) tests, 1.08 MPa and EPRI (1992) tests, 0.90 MPa. These direct tensile tests point out that concrete–rock contact has a significant

**Fig. 12 a** Shear stress and normal displacement versus shear displacement—typical curves at medium scale.  
**b** Friction coefficient ( $T/N$ ) versus shear displacement—typical curves at medium scale

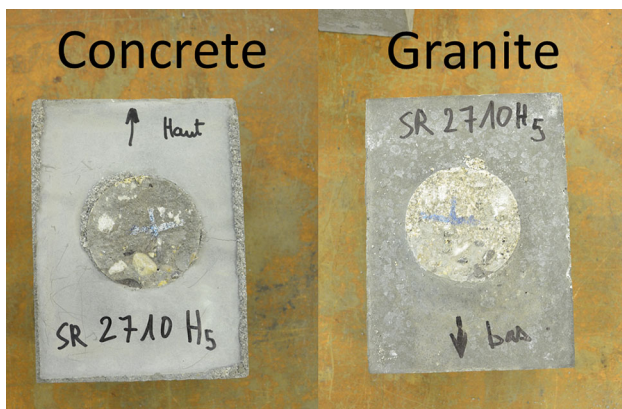
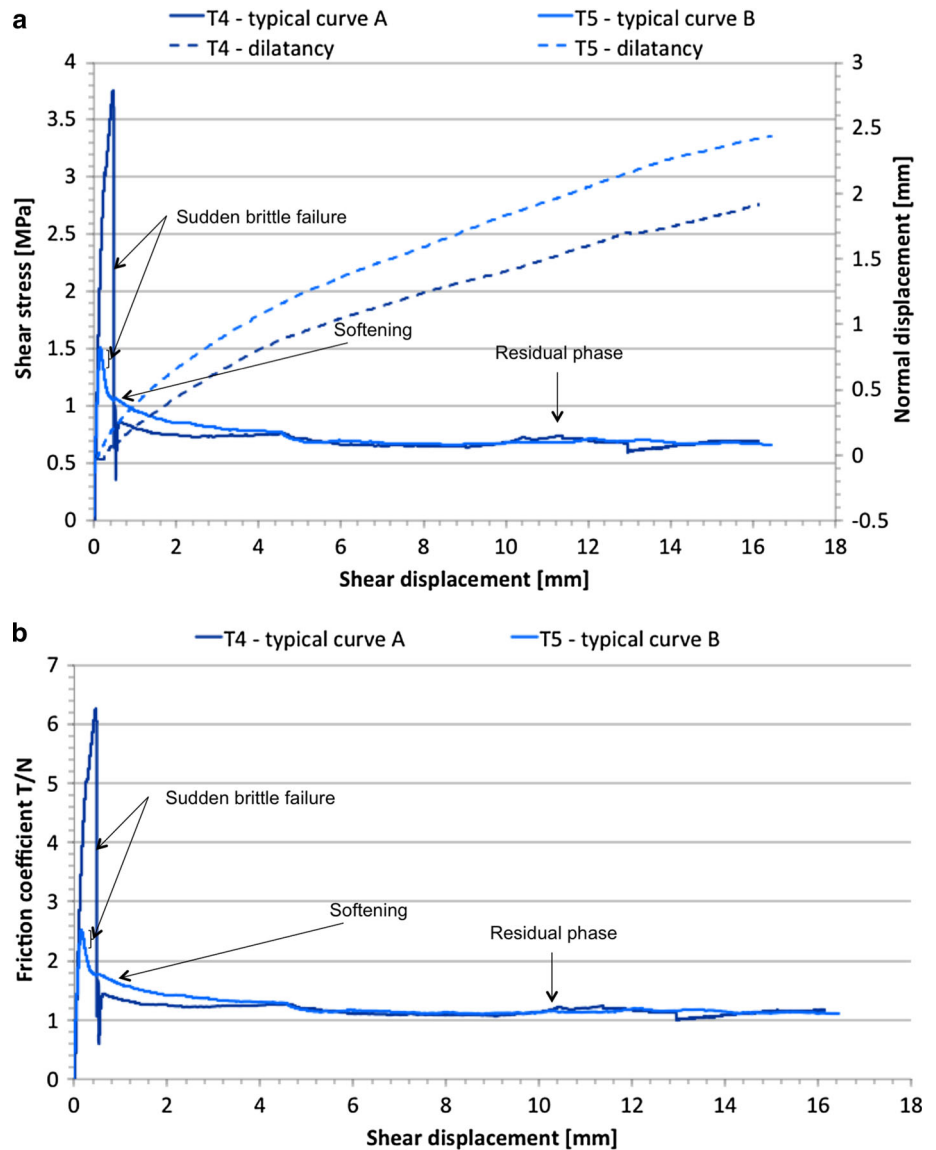
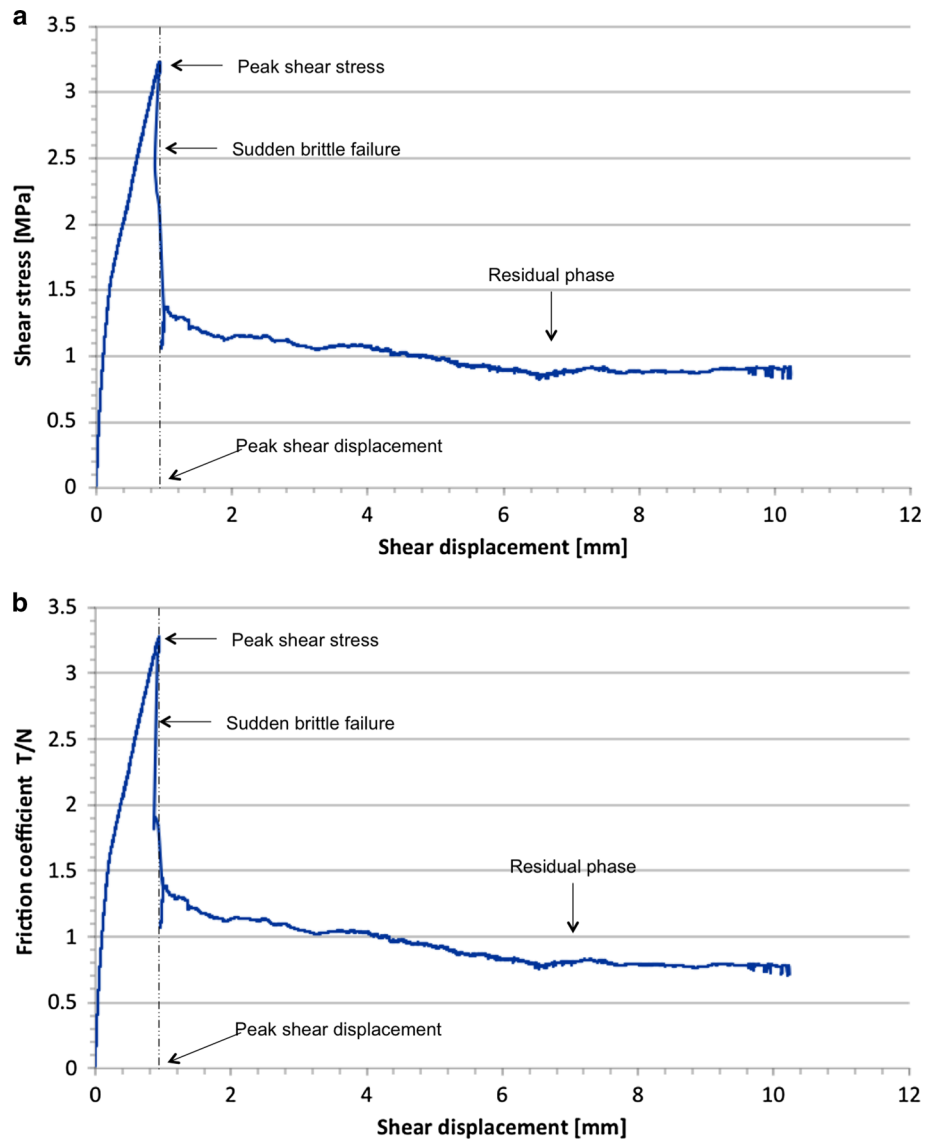


**Fig. 13** Concrete and granite surfaces of sample H5 after direct shear test. The arrows on the sample indicate the shear direction

**Table 6** Summary of the direct shear tests results at small scale

Sample	Normal stress $\sigma_n$ (MPa)	Peak shear stress $\tau_p$ (MPa)	Peak displacement $\delta_p$ (mm)	Residual stress $\tau_r$ (MPa)
H2	0.20	2.87	1.30	0.26
H7	0.20	3.08	1.06	0.25
H1	0.60	3.38	2.13	0.62
H3	0.60	2.72	1.10	0.68
H4	0.60	3.58	2.62	0.45
H5	0.60	3.51	2.45	0.48
H6	1	4.13	2.62	0.87
H8	1	3.26	0.94	0.78

**Fig. 14 a** Shear stress versus shear displacement curve for sample H8—typical curve.  
**b** Friction coefficient ( $T/N$ ) versus shear displacement curve for sample H8—typical curve



tensile strength with respect to those of concrete and rock (3.75 MPa and 10.20 MPa, respectively).

**4.4 Results Analysis**

The shear test results were linearly fitted by a Coulomb shear strength line:

$$\tau = \sigma_n * \text{Tan}(\varphi) + c$$

where  $\varphi$  and  $c$  are the friction angle and the cohesion component, respectively.

The peak shear stress as a function of the normal stress for each test and the fitted Coulomb failure criterion at small and medium scales are shown in Fig. 16. For the tested type of concrete–rock interface, the cohesion parameter value varies between 1.34 MPa and 2.78 MPa and the friction angle value between 42° and 66°. The

obtained values are consistent with values cited in the literature for concrete–granite contact (EPRI 1992:  $c = 1.26$  MPa,  $\varphi = 54^\circ$ ). In addition, comparing the values between both scales, the peak shear strength criterion varies according to the test scale as mentioned above in introduction: The cohesion component decreases with the size of sample, whereas the friction angle increases with the test scale. However, the coefficient of determination is not very high at each scale (0.372 and 0.4064).

At medium scale, this diagram emphasizes that the linear fitting of peak shear stress divides the samples into two groups which correspond to the two typical behaviors A (above the linear fitting) and B (below the linear fitting) defined in Sect. 4.1. As a matter of fact, each behavior has its own linear relationship between the peak shear stress and the normal stress (Fig. 17) within a better coefficient of determination (0.9433 and 0.708). The peak shear strength



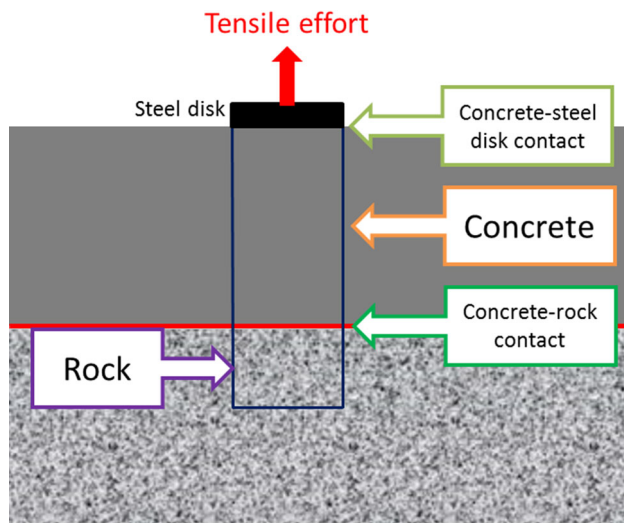


**Fig. 15** Failure locations during a direct tensile test

for the “A” behavior is higher than that of the “B” behavior. A single Coulomb criterion is thus not sufficient to characterize the concrete–rock interface shear at medium scale.

At a small scale, with respect to the Coulomb criterion, we can question the fact that the peak shear results are scattered. The study of the rock surfaces morphology of cored samples showed that all rock surfaces had similar morphologies according to statistical or three-directional parameters (Sect. 3.2). Consequently, at this scale, the scatter in results cannot be related to a morphology effect. In fact, in the sample preparation procedure, much attention was directed toward the location of the rock surface mean plane, to ensure that the shear plane of direct shear test apparatus coincides with the mean plane during the test. Figure 18 exhibits the concrete and granite surfaces of a sheared interface (cored sample H2). The concrete

surface is at the same level as the setting mortar indicating that the concrete–rock contact was not in the middle of the free encapsulated area. Moreover, it was found after the shear tests that the samples were not precisely cored in the initial identified positions (marked by crosses on the rock surface). Therefore, the marked plane on the cored sample during the preparation is not exactly the rock surface mean plane of the sheared contact. According to Armand (2000), a wrong adjustment of the contact mean plane can explain such a scatter of results. As a result, results of usual laboratory shear tests on cored concrete–rock interfaces should be used considering the actual failure path.

Figure 19 displays the residual shear stress linear curve fitting for the three previously defined cases. The shear stress without normal stress ( $c_r$ ) is about zero for each case (0.03, 0.09 and 0.12 MPa) indicating the loose of bonding between concrete and rock. Moreover, the same size effect is observed for the residual behavior: The residual friction angle determined at small scale ( $36^\circ$ ) is smaller than that obtained at medium scale ( $\sim 45^\circ$ ). The obtained values are consistent with the values cited in the literature for concrete–granite contact (EPRI, 1992:  $c_r = 0.08$  MPa,  $\varphi_r = 35^\circ$ ). Finally we can notice that the residual strength criterion is the same for both typical behaviors at medium scale.

#### 4.5 Results Comparison with the Rock Surface Morphology Aspects

At medium scale, the shear test results underline two different shear behaviors of the concrete–rock interface. Even if both exhibit a brittle response, the interface with type B behavior has a lower peak shear value and shows a softening phase after the brittle failure. This shear behavior is similar to that of a not well-bonded contact (Moradian et al. 2012; EPRI 1992). This softening phase is also observed by Tian et al. (2015) and Saiang et al.

**Table 7** Summary of the direct shear tensile results

Cored sample	Tensile strength (MPa)	Failure location
A	0.87	Concrete–rock contact
B	1.05	Concrete–rock contact
C	1.18	Concrete–rock contact
D	1.53	Concrete–rock contact
E	1.48	Concrete–rock contact
F	1.05	Concrete–rock contact
G	0.48	In concrete
H	0.97	In concrete
I	1	Concrete–steel disk contact
J	0.93	Concrete–steel disk contact
K	1.41	Concrete–rock contact
Average (for failure in concrete–rock interface)	1.22	
Coefficient of variation	19%	

**Fig. 16** Peak shear stress versus normal stress for samples tested at each scale

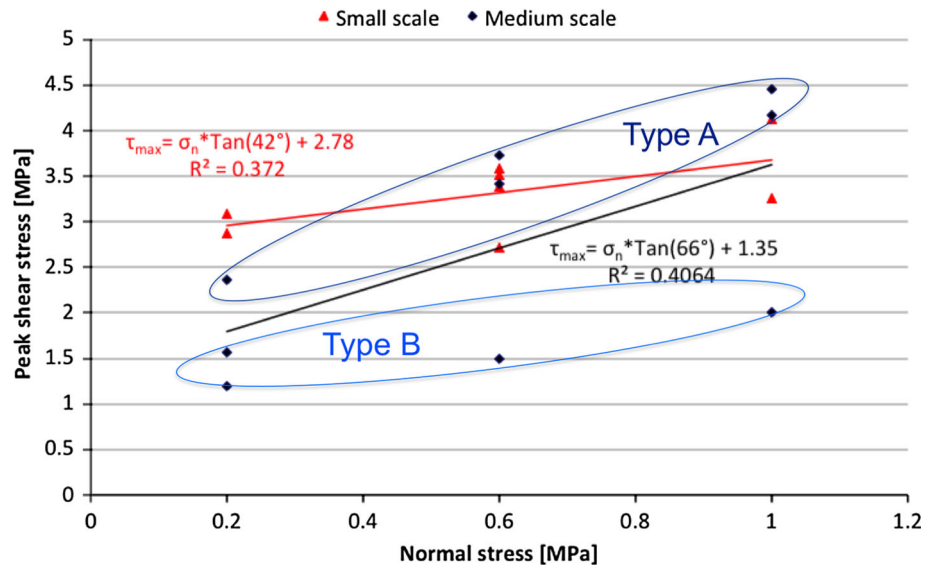
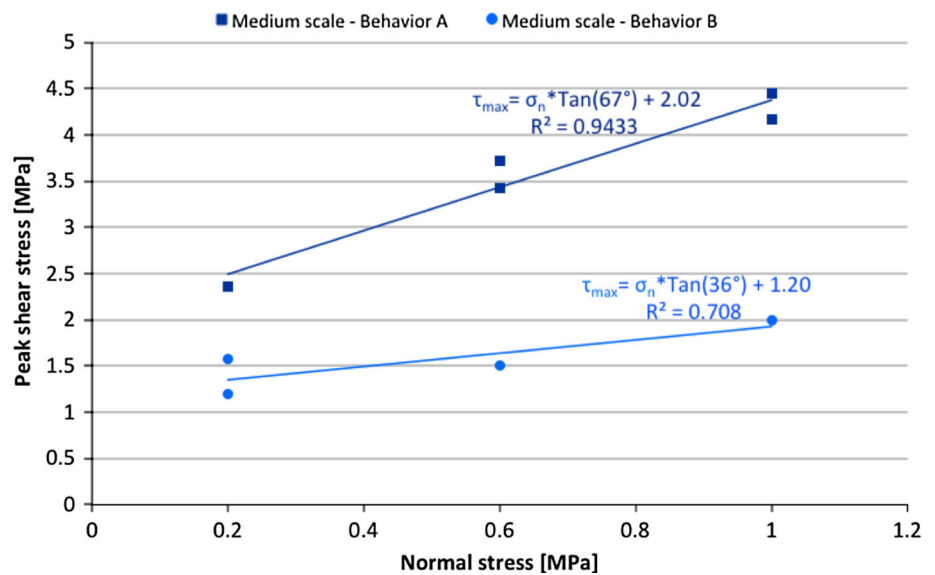


**Fig. 17** Coulomb linear curves fitting for peak shear stresses at medium scale



(2005) when the normal load is higher: They explained that the friction contributes with concrete–rock cohesion to the peak shear strength. Thus, the shear behavior of type B would be justified either by a non-uniform concrete–rock adhesion on the surface or by a non-uniform load distribution along the contact. The first hypothesis seems to be inconsistent with the results of direct tensile tests presented in Sect. 4.3. Actually the coefficient of variation on concrete–rock bond strength evaluated in different locations on 1 m<sup>2</sup> of the same concrete–rock contact was less than 20% while the evaluated cohesion parameter for type A was about 160% of that for type B. This difference in cohesion cannot therefore be justified by a variability of the initial adhesion.

Moreover, comparing the morphology aspects of the granite surfaces for each type (Fig. 20), if the magnitude of

the irregularities is the same for both behaviors, some differences can be underlined under low normal load ( $\sigma_n \leq 0.6$  MPa):

- for shear behavior A: As shown in Fig. 20a, d, g, the rock surface has a single central crest,
- for shear behavior B: As shown in Fig. 20b, c, e, the rock surface has many crests distributed on the rock surface.

This relationship between the rock morphology aspect and the shear behavior type is not found when the interfaces are sheared under higher normal stress (1 MPa): The three interfaces sheared under 1 MPa of normal stress present a rock morphology with many crests distributed on the rock surface (Fig. 20f, h, i) and only sample T8 displays a shear behavior of type B.

Under low normal load, the concrete–rock interface shear behavior seems to depend on some specificities of the rock surface morphology. The shear behavior “A” is established if the surface displays a morphology with a single central crest, i.e., in 2D simple shape, a single wave with large wave length (Fig. 21). In this case, the concrete–rock adhesion of the regular surface is mobilized uniformly on the whole interface. If the surface shows a morphology with many distributed crests, i.e., many superposed different waves or a single wave having small wave length (Fig. 22), the shearing process leads to the shear behavior “B.” The uniform establishment of the load on the whole interface is not permitted by the irregularities on the rock surface and the different stiffness between the rock and concrete. To conclude, the knowledge of the main wavelengths characterizing the rock surface roughness seems to be important to determinate the concrete–rock interface shear strength. As presented in Sect. 3.2, the usual studied roughness parameters cannot quantify a difference between

the morphologies of the 9 studied rock surfaces at this scale. In addition, they do not allow the difference between the rock surface morphology waviness to be characterized. Therefore, such a study of morphology wavelengths characterization is currently unusual.

Among the usual roughness parameters (statistical and three-directional parameters) calculated for the rock surface of samples tested at medium scale (Sect. 3.2), a substantial correspondence between the  $\theta^+$  parameter and the dilatation angle in the residual phase was underlined as shown in Fig. 23: For example with sample T5, the residual dilatation angle ( $i_r$ ) along residual phase is  $6.17^\circ$  which equals to the calculated inclination angle  $\theta^+$ . The  $\theta^+$  parameter corresponds to the mean value of the slope angle of facets which are facing the shear direction. Table 8 summarizes the obtained values. The residual shear behavior is strongly dependent of the rock surface morphology. We can confirm that during the residual phase, the concrete–rock contact has a purely frictional behavior dependent only on the mean slope value of the rock area facing the shear direction.

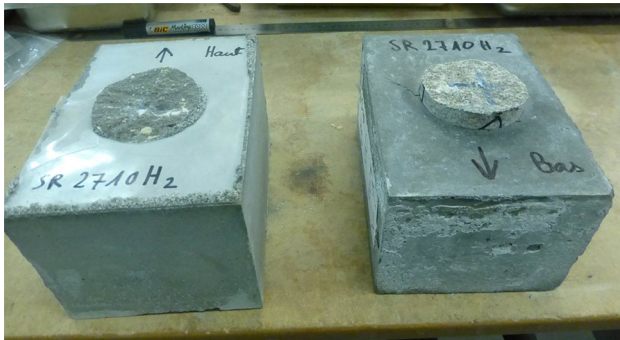
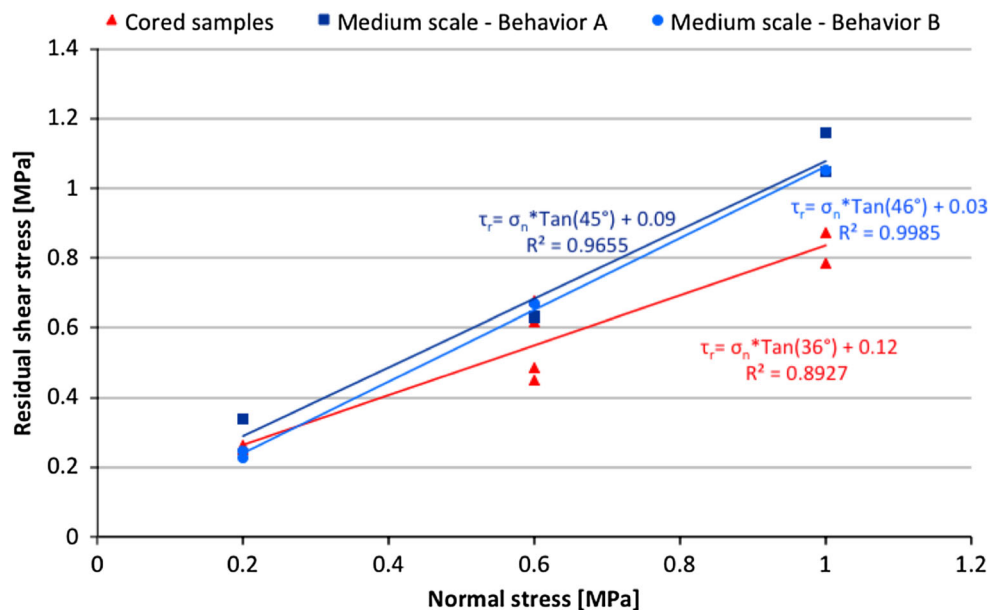


Fig. 18 Concrete and granite surfaces after shearing sample H2

### 5 A New Rock Surface Morphology Characterization Tool

The experimental shear results at medium scale underline that the concrete–rock interface shear behavior is strongly dependent on the rock surface morphology and more specifically, the waviness on the surface. To characterize the rock surface waviness, a new description tool was implemented. The method is based on the decomposition into sinusoidal functions of the rock surface morphology.

Fig. 19 Coulomb linear curve fitting for residual shear strength





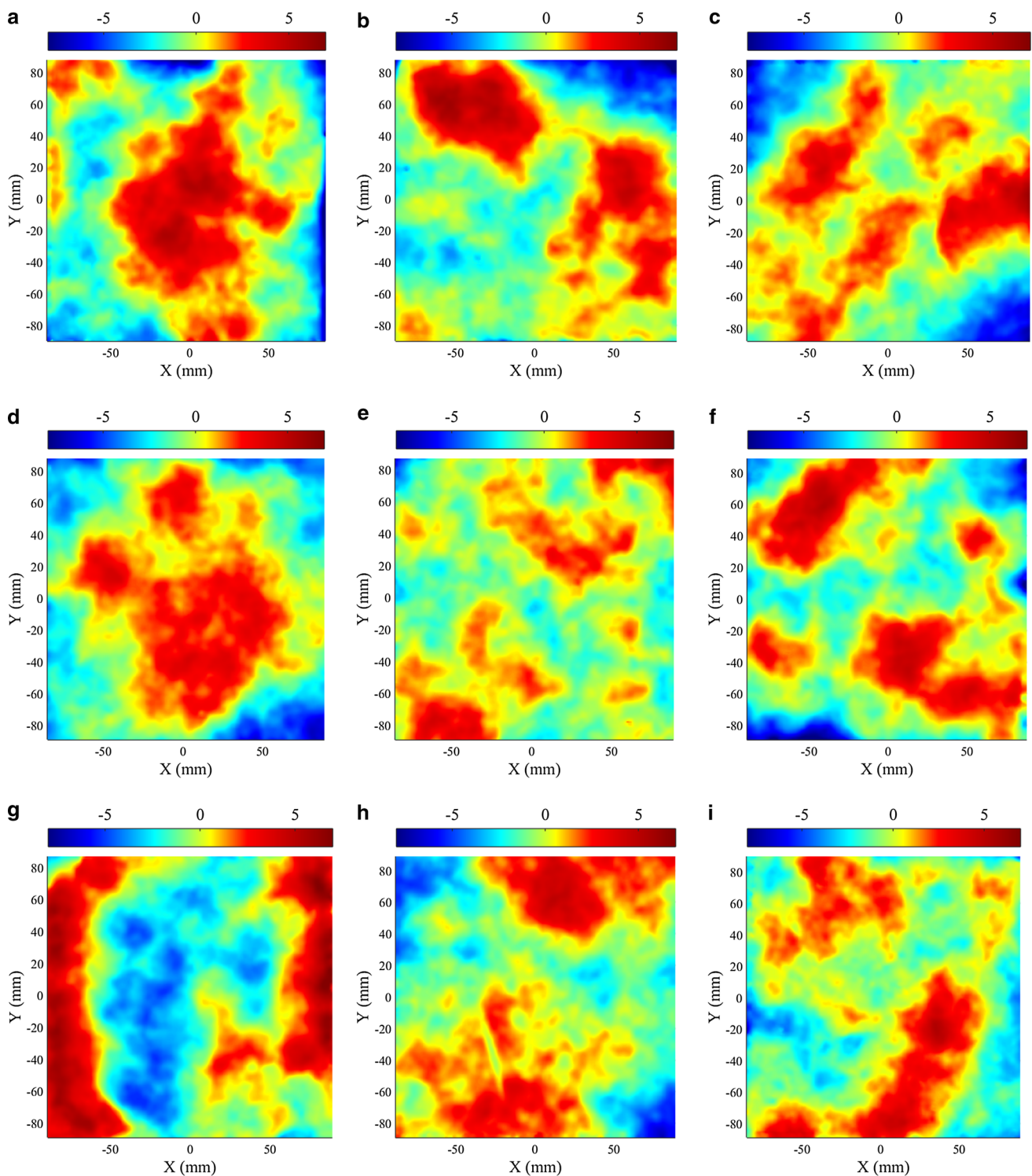


**Fig. 20** Rock surface topography of the different samples tested at medium scale. **a** Sample T1,  $\sigma_n = 0.2$  MPa—type A. **b** Sample T2,  $\sigma_n = 0.2$  MPa—type B. **c** Sample T3,  $\sigma_n = 0.2$  MPa—type B. **d** Sample T4,  $\sigma_n = 0.6$  MPa—type A. **e** Sample T5,  $\sigma_n = 0.6$  MPa—

type B. **f** Sample T6,  $\sigma_n = 1$  MPa—type A. **g** Sample T7,  $\sigma_n = 0.6$  MPa—type A. **h** Sample T8,  $\sigma_n = 1$  MPa—type B. **i** Sample T9,  $\sigma_n = 1$  MPa—type A

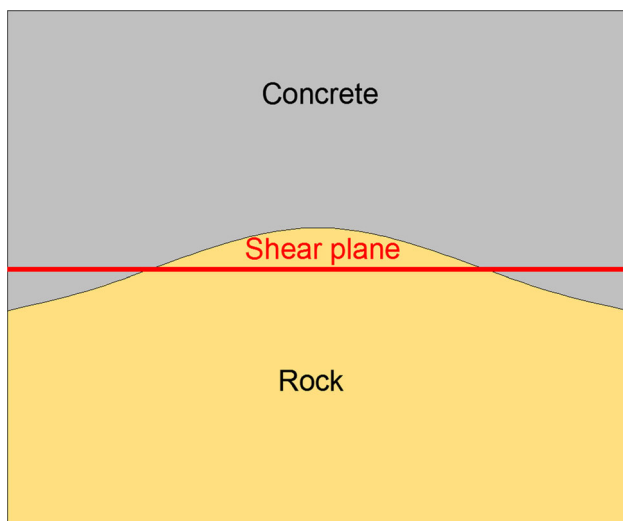


**Fig. 21** 2D layout for rock surface roughness of a shear behavior type “A”

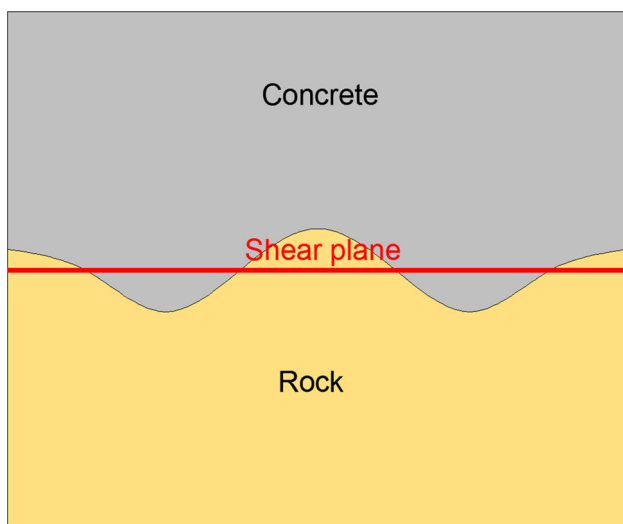


**Fig. 22** 2D layout for rock surface roughness of a shear behavior type “B”

### 5.1 Principle

The software OriginPro (OriginLab 2016) was used in this study to characterize the rock surface using cosine functions by performing a nonlinear fitting of the rock surfaces.

The fitting function created for this study was:

$$Z = f(X, Y, a, b, \lambda_1, \lambda_2, \varphi_1, \varphi_2) \\ = a * \cos\left(\frac{2\pi X}{\lambda_1} + \varphi_1\right) + b * \cos\left(\frac{2\pi Y}{\lambda_2} + \varphi_2\right)$$

where

$$X = x * \cos(\theta) + y * \sin(\theta)$$

$$Y = -x * \sin(\theta) + y * \cos(\theta)$$

and in which

- $Z$  is the altitude of the adjusted surface with respect to the mean plane;
- $X$  and  $Y$  are the coordinates obtained from a rotation of the  $x$  and  $y$  coordinates axis parallel to the sample sides, to identify a possible principal direction ( $X$ ) of the main waviness, with orientation  $\theta$  relative to the shear direction (Fig. 24);
- $\lambda_1$  and  $\lambda_2$  are the principal and secondary wavelengths in the directions  $X$  and  $Y$ , respectively;
- $a$  and  $b$  are the associated amplitudes in each direction;
- $\varphi_1$  and  $\varphi_2$  are the phase shifts in each direction.

This was a multiple nonlinear regression problem which may be expressed as follows:

$$z = f(x, y, \beta) + \varepsilon$$

with:

- $z$ , the actual elevation at a point of the surface with respect to the mean plane,
- $\beta$ , the unknown parameters,
- $\varepsilon$ , the residue between actual elevation and fitted surface.

The purpose of the nonlinear fitting is to estimate the values of the unknown parameters. The classic way to find the best-fitting surface is to seek the parameters that minimize the residue between the actual surface and the adjusted surface. Thus, the least square method was chosen. The Levenberg–Marquardt algorithm (L-M) was used as iterative procedure to assess the parameters.

### 5.2 Application on the Granite Surfaces Tested at Medium Scale

The new surface morphology characterization tool was applied to the rock surface tested at medium scale. After each application, the obtained fitted surface was compared to the actual surface, to check whether the result was acceptable or not. In some cases, the fitted surface did not well describe the actual rock surface. It turns out that the fitting method is highly dependent on the initial values of the parameters  $\beta_k$  and on the bounding values imposed to the parameters  $\lambda_1$ ,  $\lambda_2$  and  $\theta$ . Particular attention should be paid to these three parameters. No rational approach was found to select the initial values and the bounds of these three parameters. However, reasonable values may be introduced considering the aspect of each surface to be characterized. For example, to apply this description tool to the surface of interface T5 is shown in Fig. 20e which presents several peaks with a principal direction along the

**Fig. 23** Normal displacement versus shear displacement for sample T5

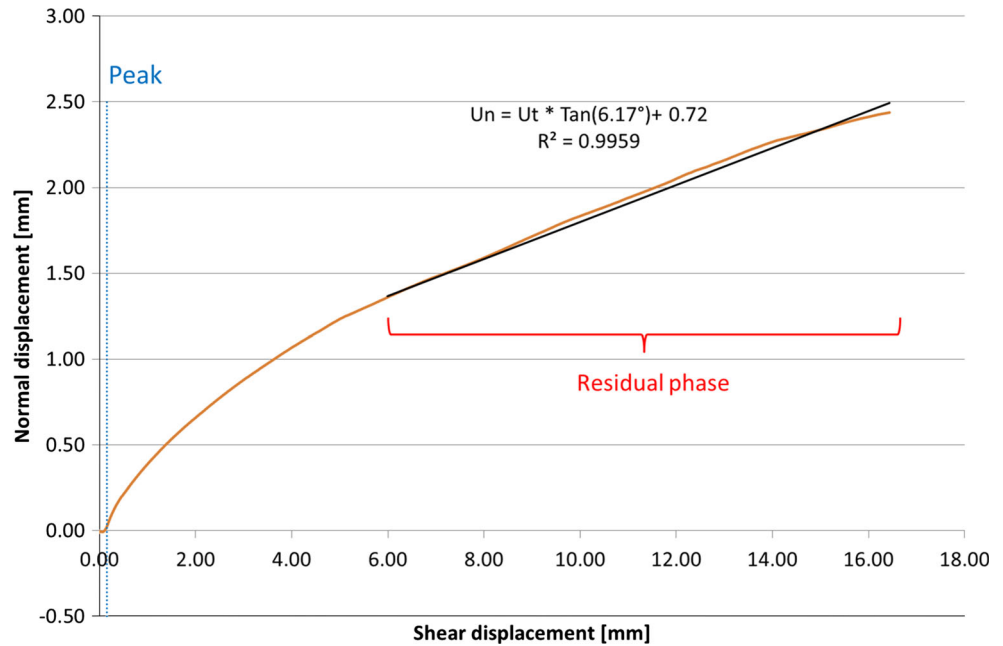


**Table 8**  $\theta^+$  angle and residual dilatation angle for the rock surface of samples tested at medium scale

Sample	Behavior	$i_r$ (°)	$\theta^+$ (°)
T1	A	10	9
T2	B	7	7.11
T3	B	–	5.96
T4	A	5.90	6.16
T5	B	6.21	6.15
T7	A	7.70	8.58
T6	A	7.10	7.48
T8	B	5.70	6.33
T9	A	6.15	6.98

diagonal of the rock surface, these different constraints were taken in the calculation process as follows:

- the orientation angle  $\theta$  was limited between  $30^\circ$  and  $60^\circ$  and the initial value was  $30^\circ$ ;
- the principal wavelength  $\lambda_1$  was limited between 25 and 60% of the surface diagonal length, i.e., between 60 and 150 mm and the initial value was 60 mm;
- the secondary wavelength  $\lambda_2$  was limited between 50 and 120% of the surface diagonal length, i.e., between 120 and 300 mm and the initial value was 120 mm.

Table 9 summarizes the parameters  $\theta$ ,  $\lambda_1$  and  $\lambda_2$ , for the new morphology characterization on the 9 rock surfaces tested at medium scale. The applied normal stress during shear test on the sheared interface and the observed shear behavior are also indicated.

For the interfaces tested under low normal stress ( $\leq 0.6$  MPa) and sheared with type A shear behavior (T1, T4 and T7), the principal direction is oriented along the shear direction ( $\theta = 0^\circ$ ) and the principal wavelength ( $\lambda_1$ ) varies between 163 mm and 192 mm, i.e., between 90 and 110% of the surface length ( $L = 180$  mm). In the secondary direction, the secondary wavelength ( $\lambda_2$ ) varies between 157 and 188 mm, i.e., in the same order of magnitude as surface width ( $W = 180$  mm).

For the interfaces tested under low normal stress ( $\leq 0.6$  MPa) and sheared with type B shear behavior (T2, T3 and T5), the principal direction is not following the shear direction, but it is inclined with angle ( $\theta$ ) varying between  $16^\circ$  and  $52^\circ$ . The principal wavelength ( $\lambda_1$ ) varies between 82 and 120 mm, i.e., between 45 and 67% of the surface length ( $L$ ). In the secondary direction, the secondary wavelength ( $\lambda_2$ ) varies between 174 and 202 mm, i.e., in the same order of magnitude as surface width ( $W$ ).

Under a normal stress of 1 MPa (T6, T8 and T9), regardless of the behavior type of A or B, the principal direction is inclined to the shear direction. The surface T8 (type B) has a principal wavelength of 188 mm which corresponds to 105% of the surface length, while the surfaces T6 and T9 sheared with type A shear behavior are characterized by principal wavelengths of 107 mm (60% of  $L$ ) and 136 mm (75% of  $L$ ), respectively.

Thus, under low normal stress, a significant difference is observed on the rock surface waviness characterization according to the shear behavior. It appears that:

- if the rock surface is characterized with a principal wavelength in order of the surface size  $\pm 10\%$  oriented



**Fig. 24** Principle of the rock surface waviness characterization

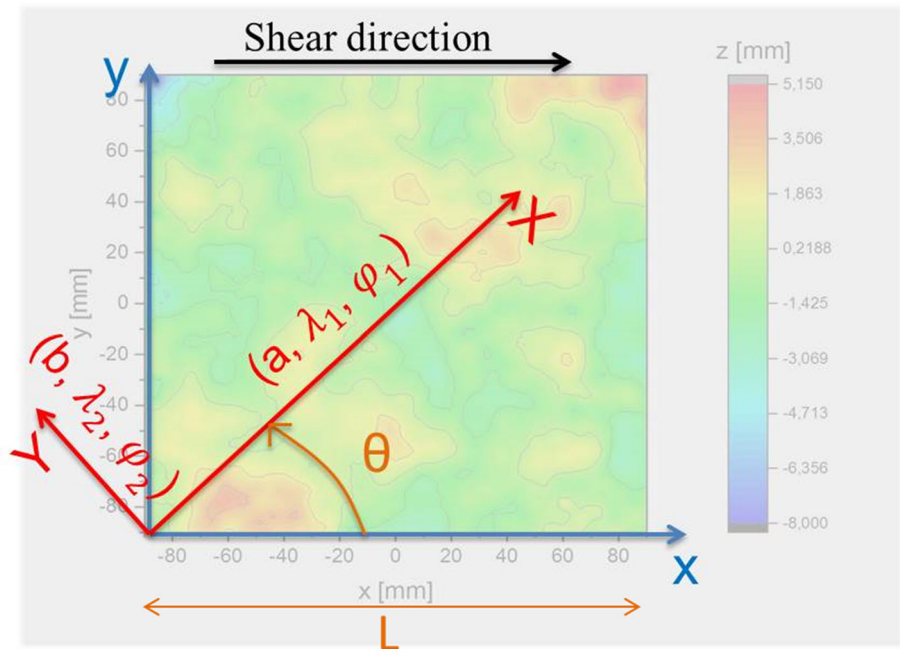


**Table 9** Summary of the new morphology characterization results for rock surfaces tested at medium scale

Surface	$\theta$ (°)	$\lambda_1$ (mm)	$\lambda_2$ (mm)	$\sigma_n$ (MPa)	Shear behavior
T1	0	163	185	0.2	A
T2	-40	113	156	0.2	B
T3	16	120	202	0.2	B
T4	0	173	188	0.6	A
T5	52	82	174	0.6	B
T6	-42	107	203	1	A
T7	0	192	157	0.6	A
T8	-20	188	176	1	B
T9	27	136	112	1	A

in the shear direction, the interface is sheared with type A shear behavior,

- if the rock surface is characterized with a principal wavelength between  $1/2$  and  $2/3$  of the surface size oriented in a direction significantly different from the shear direction, the interface is sheared with type B shear behavior.

On the contrary, this relationship between the rock waviness aspect and the shear behavior type is not considered when the interfaces are sheared under higher normal stress (1 MPa).

We may wonder if this is not only the magnitude of the principal wavelength that affects the shear behavior of the concrete–rock interface at medium scale. In fact, Khosravi

et al. (2013) emphasized, for a rock–rock interface, that the peak strength decreases when the main direction of the sawtooth asperities is inclined relative to the shear direction.

In two orthogonal directions located in the mean plane of the rock surface, the identification of a principal wavelength was sufficient to characterize the elevation with a good accuracy, compared to the actual waviness appearance of the surface. The magnitude of the principal wavelength with respect to the sample size and its orientation with respect to the shear direction allowed two classes of rock surface, which correspond to the shear failure behaviors A and B at medium scale, to be distinguished.

## 6 A Numerical Model for the Shearing of Bonded Concrete–Rock Interface at Medium Scale

In order to explain the different behaviors A and B observed at medium scale, the direct shear tests at medium scale were modeled taking into account the different surface morphologies. This numerical study was limited to the interfaces tested experimentally under low normal stress ( $\leq 0.6$  MPa), which exhibited a substantial relation between shear behavior and principal wavelength on the rock surface (Sect. 5.2). The software Abaqus (Abaqus 2012) was used for this study. This quasi-static problem was solved with an implicit analysis.

### 6.1 The 2D Numerical Model Development

Figure 25 shows the geometry and the boundary conditions of the implemented 2D model. The shear box was modeled by two steel frames having the same dimensions (internal and external) as that of the actual two half-boxes of the MTS apparatus used for the tests (Sect. 3.3.1). The free vertical spacing between the two frames was 20 mm, equal also to the actual spacing for the MTS direct shear apparatus.

The length of the concrete–rock contact was 180 mm, equal to the length of the experimentally sheared surface (Sect. 3.3.1). On both sides of the apparatus shear plane, the two materials, concrete and granite, had the same length, 180 mm in the free space and 200 mm in the area limited by the steel frames. The encapsulating material used to fill the possible gap between the sample and the half-boxes was not represented.

In order to reproduce the direct shear test conditions, the loads in the model were applied successively in two stages. Firstly, the normal load ( $\sigma_{sup}$ —Fig. 25) was gradually applied up to the value used during the test being modeled and, secondly, the tangential load was applied progressively by imposing a constant rate of tangential displacement ( $u_t$ —Fig. 25) uniformly on the left lateral side of the upper box. The bottom of the lower half-box was fixed for normal displacement and its lateral faces were fixed for tangential displacement.

In order to validate the expected influence of the rock surface main wavelength on the concrete–rock interface shear behavior under low normal stress at the medium scale, the contact surface was reproduced with the main wavelength ( $\lambda_1$ ) calculated for each surface (Sect. 5.2). The distance  $Y$  of the contact surface above or below the mean plane (which coincides with the shear plane) was characterized by the statistical parameter  $k$  (Sect. 3.2), which is the difference between the maximum and the minimum altitudes over the whole rock surface. Thus, the contact geometry was described in the model by:

$$Y = \frac{k}{2} * \cos\left(2\pi X / \lambda_1\right)$$

This model reproduces only the waviness aspect of the contact and not the asperities of the rock surface at microscale.

### 6.2 Model and Mesh for Materials

To reproduce failure within concrete and granite during direct shear test, their behaviors have to be reproduced by an elastoplastic model with damage. The elastoplastic damage model available in Abaqus is the concrete damage plasticity (CDP) model (Abaqus 2012). This model allows representing the behavior of concrete or other quasi-brittle

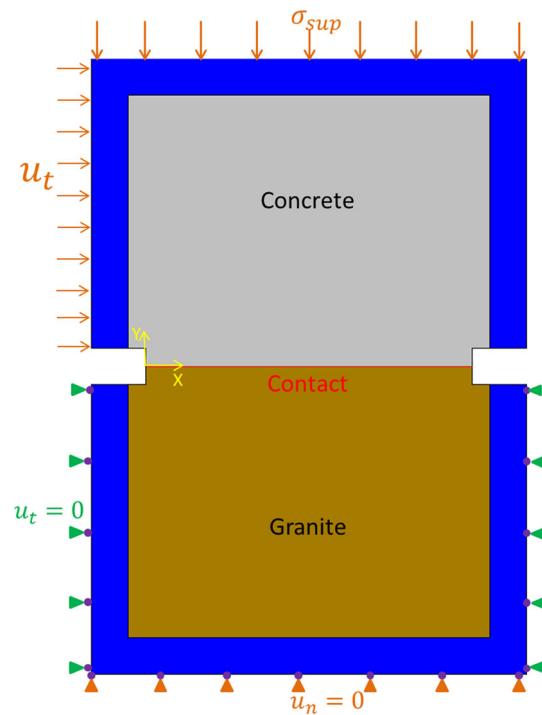


Fig. 25 Model geometry and boundary conditions

material such as granite. This model requires the knowledge of the tensile and compression behaviors of the brittle material. Based on the results of material characterization tests (Sect. 3.1) and the concrete model code 1990 (CEB-FIB 1993), both behaviors were defined for the concrete and the granite used in this study.

In order to reproduce the high stiffness of the shear box, the behavior of steel material was represented in Abaqus by a linear elastic model with high value of Young’s modulus ( $E = 193$  GPa according to Tatone and Grasselli 2012).

In a numerical model, the fineness of the mesh has an influence on the results. The easiest method to find the appropriate mesh size is to refine the mesh and run again the analysis with the new finer mesh. Once the calculations become similar, meshing with the largest size is adequate for the model. By applying this method, we found that a size of 4 mm elements was appropriate for this model.

### 6.3 Bonded Concrete–Rock Contact Model

The contact between concrete and rock was treated as an interaction between two different solids. The contact conditions were represented by a cohesive–friction model. The typical contact tangential behavior was divided into three stages:

- elastic stage: If the contact bond is undamaged, it is assumed that the cohesive part of the model is active and the friction part is ignored. Any possible local

tangential “slip” at the contact between the two solids is assumed to be purely elastic and is governed by the cohesive strength of the bond;

- bond degradation stage: If bond degradation occurs, the cohesive contribution to the shear stress along the contact starts degrading with damage evolution. Once adhesion starts degrading, the friction part of the model is activated and begins contributing to shear strength. This contribution of the friction part is progressively increased in proportion to the degradation of the cohesion part. Prior to the ultimate failure of the bond, the shear stress results from a combination of cohesion and friction contributions;
- friction sliding stage: Once the bond is completely degraded, the cohesive contribution to the shear stresses is null and the only contribution to shear strength results from friction contact conditions.

Abaqus (2012) and Tian et al. (2015) give more details about this contact model.

#### 6.4 Input Parameters Identification

The bond degradation stage in the model requires the identification of the contact cohesion ( $t_s^0$ ), the contact tensile strength ( $t_n^0$ ), the normal and tangential stiffnesses ( $K_n^c$  and  $K_s^c$ ) and the damage parameter  $D$  which describes the degradation of the bond (due to shear or tensile forces).  $D$  has an initial value of 0 when the bond is undamaged and a maximum value of 1 when the bond is totally broken. The friction sliding step in the model requires also the identification of the friction coefficient  $\mu$ .

The purpose of this study is to simulate both types of shear behavior observed at medium scale taking into account the rock surface morphology on contact. For this reason, two reasonable assumptions were formulated:

- the input parameters of the contact model are the same in both numerical models,
- these parameters are determined from the experimental study on cored samples, assuming that the local failure at medium scale is characterized by the shear and tensile strengths observed in laboratory tests on small scale samples.

The values of input parameters for the contact condition model are given in Table 10.

Furthermore, the damage initiation criterion, which defines the bond degradation initiation at a point of the contact, should be specified. The maximum stress criterion was chosen. Damage is assumed to initiate when the contact stress reaches the contact cohesion in shearing or the contact tensile strength in tension:

$$\max \left\{ \frac{\langle t_n \rangle}{t_n^0}, \frac{t_s}{t_s^0} \right\} = 1$$

where  $t_n$  and  $t_s$  are the local normal and shear stresses at a point of the contact, respectively. The symbol  $\langle \rangle$  represents the Macaulay bracket, so that a purely compressive displacement (i.e., a contact penetration) or a purely compressive stress state initiates no damage.

The model implementation needs also a damage evolution function. This function was established according to the typical shear curve obtained at small scale (Fig. 14a): The damage parameter  $D$  was described by a linear function from 0 to 1 and for which the bond is totally degraded after a shear displacement equal to 0.1 mm.

#### 6.5 Numerical Results for Direct Shear Test Simulation

The performed calculations simulated the direct shear tests on the six concrete–rock interfaces which were tested at low normal stress ( $\leq 0.6$  MPa). In the following, a typical example of the numerical results is presented for each type of interface shear behavior (A and B). Both presented here were tested under the same normal stress (0.6 MPa).

To identify the different failure mechanisms occurring at the interface during the shearing process, the local stress distributions were examined at several points along the contact. At each point, the local normal and shear stresses were calculated. Principal stresses in the solid elements adjacent to the point at the contact were also determined to investigate possible failure mechanisms in the contact materials.

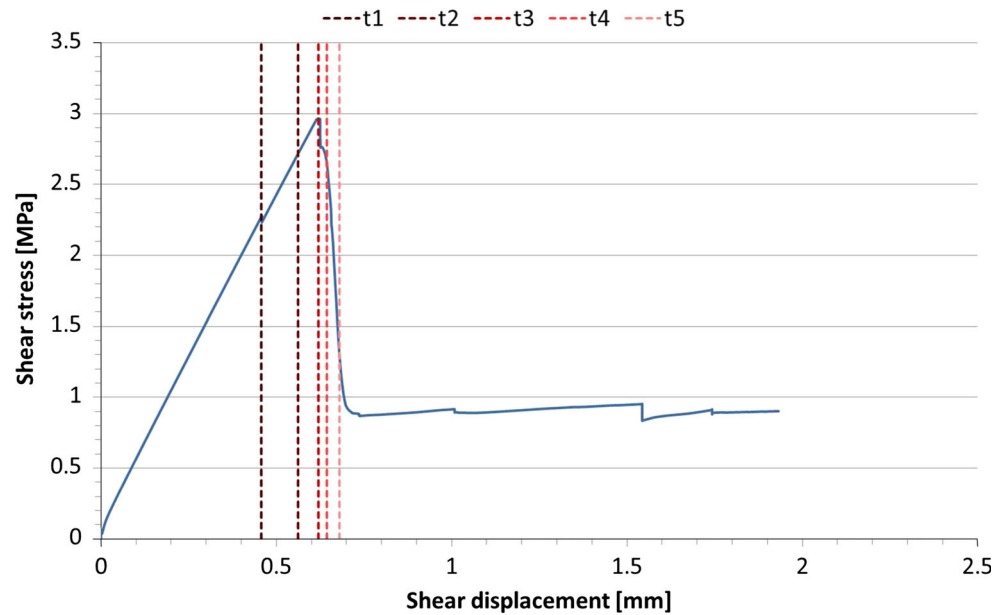
##### 6.5.1 Type A Shear Behavior, Interface T4

Figure 26 shows the average shear stress versus shear displacement curve obtained by numerical simulation on interface T4. The vertical dotted lines correspond to different times at noteworthy stages during the shearing process. A peak occurred at time  $t_3$  under a shear stress of

**Table 10** Input parameters for contact condition model

Cohesion $t_s^0$ (MPa)	Tensile strength $t_n^0$ (MPa)	Friction coefficient $\mu$	Normal stiffness $K_n^c$ (MPa/mm)	Tangential stiffness $K_s^c$ (MPa/mm)
2.8	1.2	0.9	5	5

**Fig. 26** Shear stress versus shear displacement obtained numerically for interface T4



3 MPa which is the order of peak magnitude observed for the samples displaying type A behavior.

Figure 27 summarizes the analysis of the progressive failure mechanism which occurred along the interface T4 corresponding to type A shear behavior, during the direct shear test. The failure of the concrete–rock interface began with a tensile failure in concrete on the push side (time  $t_1$ ). This failure is marked by a small peak on the global shear stress curve. It is interesting to notice that such a failure was observed during the experimental shear tests on this type of interface shear behavior. After the new distribution of stress along the interface, the concrete–rock contact began to lose its bond under shear gradually according to the shear direction (time  $t_2$ ). The friction process was initiated in the area of the contact facing the shear direction (uphill slope), where normal stress was significantly increased. The brittle failure of the concrete–rock interface (time  $t_3$ ) occurred when the contact areas quasi-parallel to the shear direction (at the top of the wave and on the opposite of the push side) reached the cohesion limit under shear. Thereafter, the contact bond was completely broken when shear stress in the area of the contact in the shear direction reached the contact cohesion limit (time  $t_4$ ). Friction mechanism kept only in the area of the contact facing the shear direction (time  $t_5$ ).

#### 6.5.2 Type B Shear Behavior, Interface T5

Figure 28 shows the average shear stress versus the shear displacement curve obtained by numerical simulation on interface T5. The vertical dotted lines correspond to

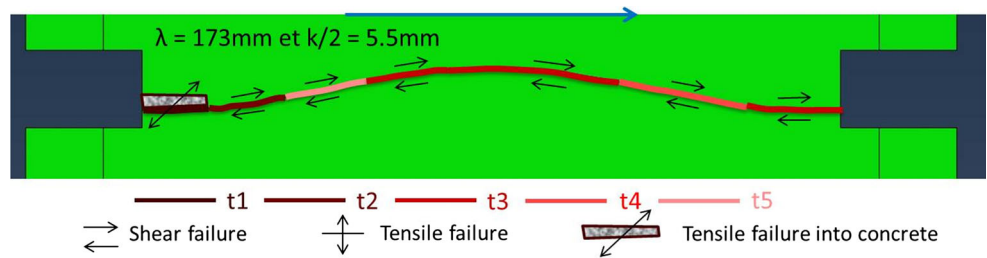
different times at noteworthy stages during the shearing process. At time  $t_1$ , the average shear stress stabilizes at a constant value equal to 2 MPa, significantly lower than the peak value of 3 MPa reached in the simulation of the shear test on the contact T4 previously presented. This stress plateau is followed by a total interface failure at time  $t_5$ .

Figure 29 summarizes the analysis of the progressive failure mechanism which occurred along the interface T5 corresponding to type B shear behavior, during the direct shear test. The failure of the concrete–rock interface began with the debonding of the contact under tensile normal stress on both downhill slopes of the contact in the shear direction (time  $t_1$ ). After the complete debonding along these two areas, the global shear stress exhibits a plateau. This plateau ends with debonding under the tensile stress of the contact area on the push side (time  $t_2$ ). Then, after the new distribution of stress along the interface, the concrete–rock contact began to lose its bond under shear gradually according to the shear direction (time  $t_3$  and time  $t_4$ ). The friction process was initiated in the area of the contact facing the shear direction (uphill slope), where normal stress was significantly increased. The brittle failure of the concrete–rock interface (time  $t_5$ ) occurred when the last contact area quasi-parallel to the shear direction (on the opposite of the push side) reached the cohesion limit under shear. Thereafter, friction mechanism kept only in the area of the contact facing the shear direction (time  $t_6$ ), where normal stress was compressive.

The global shear stress plateau simulated for T5 interface corresponds to the progressive softening phase observed in tests on interfaces exhibiting type B shear behavior (Fig. 12).



**Fig. 27** Gradual failure mechanisms for the interface T4. The arrow corresponds to shear direction



**Fig. 28** Shear stress versus shear displacement obtained numerically for interface T5

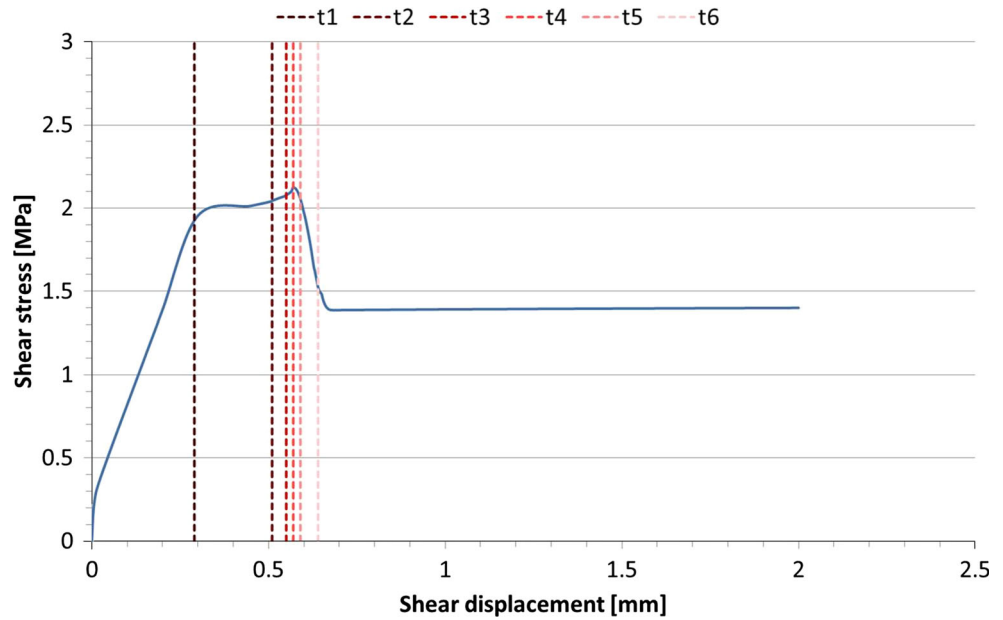
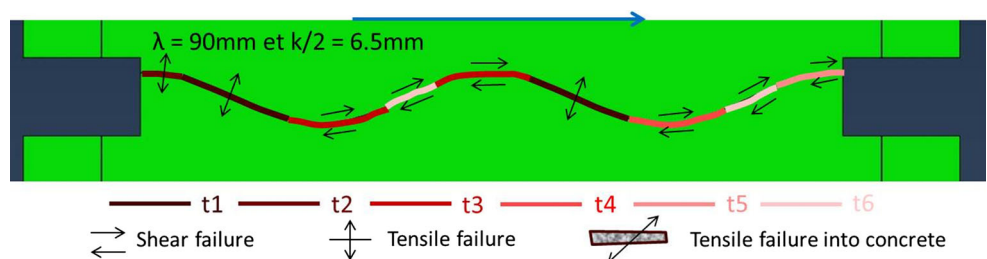


**Fig. 29** Gradual failure mechanisms of the interface T4. The arrow corresponds to shear direction



**6.6 Results Analysis**

According to the numerical model, the obtained peak shear strength for type A shear behavior (3 MPa) is significantly higher than that obtained for type B shear behavior (2 MPa). This trend is similar to the one observed experimentally. It could be justified by the fact that both shear behaviors A and B are distinguished by the failure mode that occurred along the interface:

- for type A shear behavior, despite the tensile failure in concrete on the push side, failure occurs by shearing the bond relatively uniformly along the contact. Thus, the shear strength is governed by the cohesion value on the concrete–rock contact;

- for type B shear behavior, the failure initiates by tensile debonding on the downhill slopes. Thus, the shear strength is governed by the tensile strength of the concrete–rock contact. Then failure occurs by shearing the bond more gradually along the contact.

The numerical results are consistent with the experimental results. However, comparing the peak shear strength values obtained numerically and experimentally for interfaces T4 and T5, we can notice that the numerical model underestimates by 20% the peak shear strength of interface T4 obtained experimentally (3.75 MPa) and overestimates by 30% the peak shear strength of interface T5 obtained experimentally (1.5 MPa). The fact that the implemented model is a 2D model can justify this gap

between peak shear strength values. The 3D rock surface characterization and specially the orientation of the rock surface principal wavelength ( $\theta$ ) were not considered in our model.

## 7 Discussion

### 7.1 The Effect of Rock Surface Morphology on Concrete–Rock Interface Shear Strength

At medium scale, the shear test results underline two different shear behaviors of the concrete–rock interface. Under low normal stress ( $\leq 0.6$  MPa), the new proposed characterization tool of the rock surface demonstrates the systematic relationship between the shape of the surface (waviness appearance) and the shear behavior at failure in direct shear test. The concrete–granite interface with a surface characterized by a principal wavelength in the range of the surface length ( $L \pm 10\%$ ) oriented in the shear direction will have a type A shear behavior. If the concrete–granite interface has a rock surface characterized by a principal wavelength ranging from  $1/2$  to  $2/3$  of the surface length  $L$  in a direction significantly different from the shear direction, its shear behavior will be of type B.

The results of the developed 2D numerical model are consistent with the conclusions from the experimental testing program at medium scale. Under low normal stress, the shear behavior analyzed in direct shear tests depends significantly on the main wavelength representing the contact surface compared to the length of the sample. For the same order of the contact altitude magnitude, varying the wavelength magnitude creates a different stress distribution along the interface and thus contributes to a dissimilar failure mode: For type A, the failure occurs by shearing the bond relatively uniformly along the contact, but for type B, the failure occurs more gradually by shearing along the contact after tensile debonding locally on the contact.

Since, for the same order of the altitude magnitude, the wavelength is greater for type A than for type B interfaces, the distortion angle (inclination angle of downhill slopes) for type A interfaces is lower than that of type B. In fact, when the distortion angle is large, on the contact downhill slopes, the local normal tensile stress resulting from the global applied tangential force is significant and may reach the concrete–rock contact tensile strength. When this angle decreases, for the same value of the global applied tangential force, the local normal tensile stress on these downhill slopes is lower. In this case, the local shear stress increases more significantly with increasing the global tangential force until shearing the contact bond. As a consequence, it is suggested that a minimum value of the

distortion angle exists, below which the failure mode is type A. The value of shear strength then essentially depends on the value of normal stress, which governs the local failure mode along the contact surface (cohesive–friction behavior). Above this minimum value of the distortion angle, the failure mode of the sample is type B. The value of shear strength then depends on both the normal stress and the distortion angle. For low normal stresses, an increased distortion angle will reduce the value of peak shear strength.

### 7.2 The Relationship Between Concrete–Rock Interface Cohesion Parameter and Concrete–rock Contact Tensile Strength

According to the cohesion parameter values, for samples at small scale and samples of type A at medium scale, the cohesion parameter is of the order of twice the evaluated concrete–rock contact tensile strength. The Griffith failure criterion (Curtis 2011) showed also this observation on brittle materials.

For samples of type B at medium scale, the lower value for the cohesion parameter shows that the bonding between concrete and rock is not fully loaded by shearing. In fact, in this case, the cohesion parameter is of the order of the evaluated concrete–rock contact tensile strength. This observation is consistent with the numerical analysis results insofar the shear failure for concrete–rock interface of type B begins with local contact tensile failure.

Moreover, the concrete–rock tensile strength depends on adhesion which is the fact that the cement paste in concrete is able to adhere to the underlying rock (Ruggeri et al. 2004). Therefore, concrete–rock apparent cohesion at zero normal load is strongly dependent on adhesion.

### 7.3 The Size Effect on Concrete–Rock Interface Shear Strength

Comparison between the tests at small scale and at medium scale underlines that for a concrete–rock interface, the cohesion parameter and friction angle decrease and increase with the sample size, respectively. Our numerical analysis emphasizes that the cohesion parameter depends on the rock surface morphology. As the rock surface roughness is submitted to its own size effect (Cravero et al. 1995; Tatone and Grasselli 2013), it could justify that the size effect is also more substantial for cases in which irregular morphology contributes strongly to shear strength.

In addition, according to our direct shear test results at both scales, concrete–rock interface shear failure occurs progressively at the concrete–rock contact under shear load

according to the rock surface morphology. Shear behavior at medium scale can be numerically reproduced using the results of shear behavior at small scale as local behavior. For the rock surface tested here, the medium scale seems to correspond to the representative elementary surface at which the shear strength of the principal morphology wavelength can be evaluated. Further experiments at a larger scale could complete this work to confirm the scale effect on the concrete–rock interface shear strength.

## 8 Conclusions

Direct shear tests on concrete–rock contact were performed with two different sizes of sample under normal stress range among 0.2 and 1 MPa. The sample failure happened well along the contact between concrete and rock. The strength of concrete–rock contact was actually loaded during these tests.

In this study, we point out the evaluation of a concrete–rock interface shear strength without considering concrete–rock bond leads to significantly underestimate the interface shear resistance at gravity dam foundations.

For condition under low normal load, we observe empirically that the peak shear strength is due to the brittle failure of bond between concrete and rock and the residual strength results on the purely frictional behavior at the unbonded concrete–rock contact. Moreover, the distribution of the rock crests on the surface seems to affect the shear behavior of the bonded concrete–rock interface and so its shear strength. A new morphology characterization tool was proposed and allowed two types of rock surface corresponding to two different shear behaviors A and B to be distinguished.

By means of a 2D numerical model based on the principal wavelength of this new rock surface morphology characterization, the concrete–rock contact tensile and shear strength evaluated within cored samples, the two shear behaviors types A and B observed at medium scale were reproduced. The developed model allows the stress distribution and the local failure mechanisms along the interfaces to be investigated. The results exhibit that according to the morphology principal wavelength, different failure mechanisms are involved: Shearing the bond controls the interface failure for type A shear behavior and tensile debonding controls the interface failure for type B shear behavior. Thus, we demonstrate the peak shear strength value depends on rock surface morphology as much as irregular rock surface does not permit to mobilize by shearing the concrete–rock cohesion of the whole interface at the same time. To conclude, even if the Mohr–Coulomb criterion seems to be a suitable failure criterion for concrete–rock interface, under low normal stress, it

needs to define beforehand the main morphology profile of the rock surface.

The scale effect study was limited to two different sample sizes in this work. To complete this investigation, direct shear tests must be performed on similar concrete–rock samples having large dimensions (metric scale) in order to test our theory on morphology effects and implement a model generalized of the scale effect phenomenon.

**Acknowledgements** This research program was made possible by the financial support of Electricité de France (EDF—French Electricity Company).

## References

- Abaqus (2012) Abaqus analysis user's manual. Dassault system. [https://things.maths.cam.ac.uk/computing/software/abaqus\\_docs/docs/v6.12/books/usb/default.htm](https://things.maths.cam.ac.uk/computing/software/abaqus_docs/docs/v6.12/books/usb/default.htm)
- Andjelkovic V, Pavlovic N, Lazarevic Z, Nedovic V (2015) Modeling of shear characteristics at the concrete–rock mass interface. *Int J Rock Mech Min Sci* 76(1):222–236. doi:10.1016/j.ijrmms.2015.03.024
- Armand G (2000) Contribution à la caractérisation en laboratoire et à la modélisation constitutive du comportement mécanique des joints rocheux. Dissertation, University of Grenoble 1, France
- Bandis S, Lumsden AC, Barton NR (1981) Experimental studies of scale effects on the behavior of rock joints. *Int J Rock Mech Min Sci* 18(1):1–21. doi:10.1016/0148-9062(81)90262-X
- Barla G, Robotti F, Vai L (2011) Revisiting large size direct shear testing of rock mass foundations. In: 6th international conference on dam engineering, Lisbon, Portugal
- Barton N, Choubey V (1977) The shear strength of rock joints in theory and practice. *Rock Mech* 10(1):1–54. doi:10.1007/BF01261801
- Bauret S, Rivard P (2015) Predicting the tensile bond strength of the concrete–rock interface through a parametric laboratory study. In: Annual conference of Canadian dam association, Mississauga, ON, Canada
- Castelli M, Re F, Scavia C, Zaninetti A (2001) Experimental evaluation of scale effects on the mechanical behavior of rock joints. In: Proceedings of Eurock 2001 rock mechanics—a challenge for society, Espoo, Finland
- CEB-FIB (1993) Model code 1990. Thomas Telford Ltd. doi:10.1680/ceb-fipmc1990.35430
- CFBR (2013) Recommendations for the justification of the stability of gravity dams. Comité Français des Barrages et Réservoirs, Justification of gravity dams work group, France
- Champagne K, Rivard P, Quirion M (2013) Paramètres de résistance au cisaillement associés aux discontinuités des barrages en béton du Québec. In: Annual conference of Canadian dam association, Montréal, Québec, Canada
- Cravero M, Iabichino G, Piovano V (1995) Analysis of large joint profiles related to rock slope instabilities. In: 8th conference of ISRM, Tokyo, Japan
- Curtis DD (2011) Estimated shear strength of shear keys and bonded joints in concrete dams. 21st Century dam design—advances and adaptations. In: 31st annual conference of USSD, San Diego, California, USA
- Deveze G, Coubarde G (2015) Développement d'une base de données sur la résistance à la traction de l'interface béton-roche. Colloque

- du comité français des barrages et réservoirs: fondations des barrages, Chambéry, France
- El-Soudani SM (1978) Profilometric analysis of fractures. *Metallography* 11(3):247–336. doi:[10.1016/0026-0800\(78\)90045-9](https://doi.org/10.1016/0026-0800(78)90045-9)
- EPRI (1992) Uplift pressures, shear strengths and tensile strengths for stability analysis of concrete gravity dams, vol 1. Electrical Power Research Institute. Prepared by stone and webster engineering corporation. Denver, Colorado
- Fardin N, Stephansson O, Jing L (2003) Scale effect on the geometrical and mechanical properties of rock joints. In: 10th conference of ISRM, Sandton, South Africa
- Gentier S (1987) Morphologie et comportement hydromécanique d'une fracture naturelle dans le granite sous contrainte normale: Etude expérimentale et théorique. Rapport de thèse, Université d'Orléans, France, p 597. No. 1986ORLE2013
- Ghosh, AK (2010) Shear strength of dam-foundations rock interface—a case study. In: Annual conference of Indian geotechnical society, Umbai, Maharashtra, India
- Grasselli G (2001) Shear strength of rock joints based on quantified surface description. Dissertation, Ecole polytechnique federale de Lausanne, Suisse
- Gutiérrez MC (2013) Shear resistance for concrete dams. Dissertation, Norwegian University of Science and Technology, Trondheim, Norvège
- Johansson F (2009) Shear strength of unfilled and rough rock joints in sliding stability analyses of concrete dams. Dissertation, Royal Institute of Technology, Stockholm, Sweden
- Khosravi A, Sadaghiani MH, Khosravi M, Meehan CL (2013) The effect of asperity inclination and orientation on the shear behavior of rock joints. *Geotech Test J* 36(3):1–14. doi:[10.1520/GTJ20120060](https://doi.org/10.1520/GTJ20120060)
- Kodikara JK, Johnston IW (1994) Shear behaviour of irregular triangular concrete–rock joints. *Int J Rock Mech Min Sci* 31(4):313–322. doi:[10.1016/0148-9062\(94\)90900-8](https://doi.org/10.1016/0148-9062(94)90900-8)
- Krounis A, Johansson F, Larsson S (2015) Effects of spatial variation in cohesion over the concrete–rock interface on dam sliding stability. *Rock Mech Geotech Eng* 7(6):659–667. doi:[10.1016/j.jrmge.2015.08.005](https://doi.org/10.1016/j.jrmge.2015.08.005)
- Krounis A, Johansson F, Larsson S (2016) Shear strength of partially bonded concrete–rock interfaces for application in dam stability analyses. *J Rock Mech Geotech Eng* 49(7):2711–2722. doi:[10.1007/s00603-016-0962-8](https://doi.org/10.1007/s00603-016-0962-8)
- Lo KY, Lukajic B, Wang S, Ogawa T, Tsui KK (1990) Evaluation of strength parameters of concrete–rock interface for dam safety assessment: session 2—Dam Safety Assessments. Canadian Dam Safety Conference, Toronto, Ontario, Canada
- Lo KY, Ogawa T, Lukajic B, Dupak DD (1991) Measurement of strength parameters of concrete–rock contact at the dam-foundation interface. *Geotech Test J* 14(4):383–394. doi:[10.1520/GTJ10206J](https://doi.org/10.1520/GTJ10206J)
- Maksimovic M (1996) The shear strength components of a rough rock joint. *Int J Rock Mech Min Sci* 33(8):769–783. doi:[10.1016/0148-9062\(95\)00005-4](https://doi.org/10.1016/0148-9062(95)00005-4)
- Moradian Z (2011) Application de la méthode d'émission acoustique pour la surveillance du comportement au cisaillement des joints actifs. Dissertation, University of Sherbrooke, Québec, Canada
- Moradian Z, Ballivy G, Rivard P (2012) Application of acoustic emission for monitoring shear behavior of bonded concrete–rock joints under direct shear test. *Can J Civ Eng* 39(8):887–896. doi:[10.1139/I2012-073](https://doi.org/10.1139/I2012-073)
- MTS (2014) MTS model 815 and 816 rock mechanics test systems. [https://www.mts.com/ucm/groups/public/documents/library/mts\\_008000.pdf](https://www.mts.com/ucm/groups/public/documents/library/mts_008000.pdf)
- Muralha J, Grasselli G, Tatone B, Blümel M, Chryssanthakis P, Yujing J (2014) ISRM suggested method for laboratory determination of the shear strength of rock joints: revised version. *Rock Mech Rock Eng* 47(1):291–302. doi:[10.1007/s00603-013-0519-z](https://doi.org/10.1007/s00603-013-0519-z)
- Myers NO (1962) Characterization of surface roughness. *Wear* 5(3):182–189. doi:[10.1016/0043-1648\(62\)90002-9](https://doi.org/10.1016/0043-1648(62)90002-9)
- OriginLab (2016) Algorithms—non linear curve fitting. <http://www.originlab.com/doc/Origin-Help/NLFit-Algorithm>
- Patton FD (1966) Multiple modes of shear failure in rock. In: 1st conference of ISRM, Lisbon, Portugal
- Ruggeri G, Pellegrini R, Rubin de Celix M et al (2004) Sliding stability of existing gravity dams—final report. ICOLD European working group on sliding safety of existing gravity dams
- Saiang D, Malmgren L, Nordlund E (2005) Laboratory tests on shotcrete-rock joints in direct shear, tension and compression. *Rock Mech Rock Eng* 38(4):275–297. doi:[10.1007/s00603-005-0055-6](https://doi.org/10.1007/s00603-005-0055-6)
- Tatone B, Grasselli G (2009) A method to evaluate the three-dimensional roughness of fracture surfaces in brittle geomaterials. *Review of Scientific Instruments* 80(12):125110-1-10. doi:[10.1063/1.3266964](https://doi.org/10.1063/1.3266964)
- Tatone B, Grasselli G (2012) Modeling direct shear tests with FEM/DEM: investigation of discontinuity shear strength scale effect as an emergent characteristic. In: Conference of American rock mechanics, Chicago, USA
- Tatone B, Grasselli G (2013) An investigation of discontinuity roughness scale dependency using high-resolution surface measurements. *Rock Mech Rock Eng* 46(4):657–681. doi:[10.1007/s00603-012-0294-2](https://doi.org/10.1007/s00603-012-0294-2)
- Tian HM, Chen WZ, Yang DS, Yang JP (2015) Experimental and numerical analysis of the shear behavior of cemented concrete–rock joints. *Rock Mech Rock Eng* 48(1):213–222. doi:[10.1007/s00603-014-0560-6](https://doi.org/10.1007/s00603-014-0560-6)
- Westberg Wilde M, Johansson F (2013) System reliability of concrete dams with respect to foundation stability: application to a spillway. *Geotech Geoenviron Eng* 139(2):308–319. doi:[10.1061/\(ASCE\)GT.1943-5606.0000761](https://doi.org/10.1061/(ASCE)GT.1943-5606.0000761)
- XP P 94-424 (2003) French standard: cisaillement direct selon une discontinuité de roche. ISSN 0335-3931